The Dissertation Committee for Walter Benjamin Fair, Jr. Certifies that this is the approved version of the following dissertation:

An Integrated Model for Production of Marginal Oil Fields

Committee:

Tadeusz W. Patzek, Supervisor

Kamy Sepehrnoori, Co-Supervisor

Eric van Oort

Jon E. Olson

An Integrated Model for Optimizing Production of Marginal Oil Fields

by

Walter Benjamin Fair, Jr.

Dissertation

Presented to the Faculty of the Graduate School of

The University of Texas at Austin

in Partial Fulfillment

of the Requirements

for the Degree of

Doctor of Philosophy

The University of Texas at Austin

May 2019

Dedication

I dedicate this work to my late parents, Walter B. Fair, Sr. and Marianne Fair, who provided a loving home while they instilled within me a love for learning and a work ethic; to my maternal grandfather, Hans A. Harrfeldt, who always encouraged me to study; to my wife Argentina Fair, who supported me throughout my studies; and to my children, step-children and grandchildren, who always offered words of encouragement and overlooked the fact that going back to school was simply a crazy thing to do for an old man.

Acknowledgements

No work can be done in isolation and this dissertation is no exception. I have certainly gained insight from many people throughout my life and it would be impossible to name all of them. I would like to express special thanks to my supervisors, Dr. Patzek and Dr. Sepehrnoori, for putting up with me and keeping me focused on the tasks at hand. As well, many discussions with Dr. M. Shirdel were very useful in trying to model transient pipe flow. Thanks also to Ample Resources, Inc. for permission to use field data to validate the work documented herein.

An Integrated Model for Optimizing Production of Marginal Oil Fields

Walter Benjamin Fair, Jr., Ph.D.

The University of Texas at Austin, 2019

Co-Supervisors: Tadeusz W. Patzek and Kamy Sepehrnoori

For the optimization of production in an operating marginal oil field, it is necessary to consider the reservoir inflow, the artificial lift systems, as well as the surface facilities. Since most reservoir simulation software does not include detailed facility modeling, an integrated model of an entire field has been developed including the surface facilities, to allow detailed modeling of the entire field operation. This model is useful for optimizing production and for use in field surveillance activities, as well as investigating the applicability of simplified engineering assumptions.

Table of Contents

Chapter 1: Introduction 1
Organization 3
Chapter 2: Oil Field Flow Network 5
Generic Field Description 6
Design Goals 7
Description of Flow Network 7
Implementation 10
Flow Network 13
Name: 13
Parameters: 13
Methods 13
Flow Equipment 14
Name: 14
Parameters: 14
Methods 14
Flow Stream 15
Name: 15
Parameters: 15
Methods 15
Chapter 3: Multiphase Pipe Flow 17
Flow Equations 18
Conservation of Mass 19
Liquid Momentum 19
Gas Momentum 19
Oil + Water Mass Balance 20
Water Mass Balance 20
Total Energy 20
Annular Flow 20

Flow Patterns 21
Fluid Drag 22
Interfacial Drag 22
Initial and Boundary Conditions 23
Solution of Flow Equations 23
Momentum Balance Equations 24
Mass Balance Equations 25
Energy Balance Equation 26
Validation 27

Chapter 4: Multiphase Separators 35
Vertical Separator 36
Fundamental Equations 36
Numerical Solution 39

Chapter 5: Well Model 42
Constant Rate Well 42
Beam Pumps 43
Rod Motion 45
Surface Pumping Unit 48
Downhole Pump 49
Casing Annulus 50
Reservoir and completion model 51

Chapter 6: Auxiliary Flow Equipment 54
Flow Junctions 54
Tanks 55
Surface Pumps 55
Compressors 55
Chokes 56

Chapter 7: Field Applications 57

Conclusions and Recommendations 62

Conclusions: 62

Recommendations: 62

Appendices 65

Appendix A1: Fluid Properties 65

Black Oil PVT Model 65

Brine 67

Composition 67

Density 67

Formation Volume Factor 68

Viscosity 68

Oil 69

Density 69

Formation Volume Factor 69

Solution Gas-Oil Ratio 70

Viscosity 70

Heat Capacity 71

Gas 71

Z Factor 72

Density 72

Formation Volume Factor 73

Viscosity 73

Heat Capacity 73

Appendix A2: Parameter Estimation 74

Heat Transfer Coefficients 74

References 77

Chapter 1: Introduction

In order to optimize production from marginal oil fields, it is necessary to consider reservoir, well, and surface facility performance. The purpose of this research is to develop a complete model for use in evaluating efficient methods for operating oil fields including marginal fields.

According to the US Department of Energy, stripper wells are defined as wells producing less than 10 barrels of oil per day. The Interstate Oil and Gas Compact Commission IOGCC (2008) reports that in 2008 there were over 396,000 stripper wells in the US producing over 291,000,000 bbl of oil and over 130,000 stripper wells producing 120,000,000 bbl of oil were in Texas. Other sources indicate that as much as 1 out of every 6 barrels of oil in the US is produced from stripper wells. In 2009, the Independent Petroleum Association of America estimated that 85% of US wells produce less than 15 bbl of oil per day and account for about 20% of the total US production. Since producing wells naturally exhibit declining production rates, more wells will inevitably be added to these numbers each year. Because of the low producing rates, most of these wells are marginally economic and since most are not operated by major companies with research facilities, there is little fundamental corporate research directly supporting development and operation of these wells. On account of the strategic importance of marginal wells and the lack of industry research, the study of these wells will be an important contribution to the energy outlook for the State of Texas and the US.

Optimizing production from such marginal wells is a daunting effort for reasons documented in the IOGCC (2008) report. In order to optimize production and ultimate recovery from an oil field, it is necessary to consider reservoir fluid flow, recovery processes, well design, artificial lift, surface facilities, operational constraints and logistical

problems. With the availability of cheap computing and communication facilities, there has been an emphasis on real-time monitoring and control where in other industries concepts such as data mining and real time analysis have been applied to great advantages. While much work has been done on each of the individual parts of this overall problem, the full integration of the parts has not generally been done, especially on a scale suitable for application to marginally economic wells and fields. In particular, it appears that most of the work toward real-time monitoring and surveillance applies mainly to larger, economically viable fields, but cannot obviously be applied to the vast majority of marginal fields and wells due to infrastructure and economic considerations. The result of this research is the development of an integrated model for use in evaluating efficient methods for operating all types of oil fields including marginal fields.

Besides the problem of integrating reservoirs, wells, surface facilities, operational and logistical systems, the relative time scale at which each subsystem operates adds additional complexity. Normally, reservoir processes may take weeks, months or years to reach steady-state conditions, while the flow in wells may stabilize in a period of hours or days. The use of beam pumps may force cycles of hours with the use of timers and pump-off controllers, while pulsating flow due to individual pump strokes can be measured in seconds. In the surface facilities, compressors and pumps respond to changes in seconds, while separators usually have residence time on the order of minutes. Since it is generally impractical to run a typical reservoir simulator with time steps on the order of minutes, seconds or less, a realistic means of scaling the time behavior of the various systems is important. It is not clear that simple time averaging of models can properly represent phenomena occurring at smaller time scales that may have an important effect on operations and economics.

Aside from the model integration challenges mentioned, the problem of optimizing production from marginal wells is a particularly complex endeavor. Low producing rates can be caused by poor reservoir quality, high fluid viscosity, low pressure, high water saturation, sand production, mechanical problems, artificial lift constraints, and other considerations. In addition, although technical solutions to the problems may be known, low rates correspond generally to low revenue that may easily make the implementation uneconomic. Furthermore, since these wells are comparatively low income producers, resources are often not spent on data acquisition. As a result, the application of technology and the acquisition of data must be based upon adding value in the presence of tight constraints on economics, expenditures and data availability.

ORGANIZATION

Since the purpose of this work is to develop an integrated model, inevitably the subjects involved will be intertwined; hence, no simple linear organization is possible. Chapter 2 presents the field network model that integrates all of the individual parts of a full field model developed in this work. The following Chapters 3, 4, and 5 present detailed models of the pipes, separators and wells that are incorporated into the integrated model, each of which presents complex modeling challenges. Chapter 6 presents a summary of auxiliary equipment models that were not modeled in detail, such as flow junctions, pumps, compressors, and tanks. Finally, Chapter 7 presents examples of the use of the model. Since fluid properties and other parameters are important in the application of the integrated model, the appendices document the fluid properties and parameters, as well as methods for estimation when data are not available.

As a result of this work, an integrated field modeling framework has been produced and implemented. The resulting software named Integrated Field Model (IFM) has been

written in C# using Microsoft Visual Studio™ that can be run on many Windows™ operating systems. The software has been tested on Windows Vista, Windows 7 and Windows 8 and Windows 10.

The purpose of this research is to develop a complete model for use in evaluating efficient methods for operating all types of oil fields including marginal fields

Chapter 2: Oil Field Flow Network

In order to represent flow in an entire field consisting of reservoirs, wells, pipes, separators, pumps, compressors, tanks, and other assorted equipment, it is necessary to develop a framework for representing the flow network and determine computational methods to solve the coupled flow equations for each entity, as well as the network as a whole. This chapter summarizes the definition of a flow network that will serve as the framework for flow calculations in the integrated field model.

To have a basis for the design and implementation of the integrated field model and to ensure that it can be applied to actual marginal fields, a generic marginal field is first defined. The defined generic field should have enough flexibility to allow representation of the majority of actual marginal fields. In order to model, history match and optimize total recovery from marginal fields, a computational framework is needed that can represent the necessary equipment and fluid flow within the wells and through the surface equipment. In order to optimize the recovery, production and operations, the framework should be capable of multiphase fluid flow calculations, allow the estimation of operating costs and be amenable to data input and output requirements. Within the overall integrated system, numerical models of each of the defined subsystems can then be developed. These will vary in complexity depending upon the detail required within the overall system model. Some modules will require detailed, finite difference representations (i.e. flowlines, separators, and reservoirs), while other modules may be simply represented by a pressure change, perhaps with computed horsepower requirements (i.e. pumps, chokes, compressors, etc.).

GENERIC FIELD DESCRIPTION

According to information provided in, as well as personal experience, a typical marginal oil field in the US consists of low-rate oil wells often with large amounts of water producing by beam pump. Flow lines connect the wells to a header where they flow into a series of separators. Gas may be produced from the casing head of the wells and taken off the separators and may be compressed for sale or field use, or in few cases be flared. In some fields, casing gas is produced through a separate compression system to reduce the bottomhole pump intake pressure and increase reservoir inflow into the wellbore. Free water is usually taken off from each separator stage and stored in a tank for trucking or be injected into a disposal well. Oil taken from the separators may require additional separation to yield acceptable quality oil for sale. Finally, the oil is held in a stock tank at atmospheric pressure and ambient temperature where it awaits sales by either a LACT unit or transportation by truck. As a result, without much loss of generality, a flow system consisting of reservoirs and wells, flowlines, various stages of separators and tanks is chosen as a typical marginal field model. A sketch of such a field flow diagram is shown in Figure 2.1. Additional reservoirs, wells, separators, pumps, compressors and chokes can be included as required in order to represent actual field operations.

The basic flow system can be represented by a network flow diagrams, which is assumed to have no cyclic paths, thus simplifying the computational procedures. If we assume that suitable check valves are installed at strategic locations (as is common to prevent backflow), this system can be represented mathematically as a directed acyclic graph, often referred to as a digraph or DAG. A mathematical abstraction of an acyclic digraph is shown in Figure 2.2. By using a mathematical abstraction to represent the flow system, many techniques from computer science (Aho et al., 1983) can be applied to represent and manipulate the network flow model.

DESIGN GOALS

To design a workable integration framework, it is useful to list the requirements a workable model would have. These requirements then serve as a guide in considering options and as a check on the feasibility of the final defined model. The design goals for the flow system model are as follows:

1. The model must be capable of representing the applicable physics of fluid flow within a typical oil field.
2. The model must be represented in a computationally efficient manner for solution on typical desktop and laptop computers.
3. The model must be extensible, so that additional equipment can be added at a later date and not be limited to flow equipment currently envisioned.
4. The model must be capable of representing arbitrary connections between equipment items so that a wide variety of configurations can be represented.
5. An algorithm based on physical considerations must be developed for solution of the overall flow network.
6. The system must provide a general means for detailed models, internal to each specific flow equipment items, to be developed.

DESCRIPTION OF FLOW NETWORK

The defined flow system used in this work is based on an abstract directed acyclic graph (Aho, 1983) where each equipment item is represented by a node and where arcs represent the flow streams or connections between equipment. This is a standard approach previously described by various authors to represent flow networks (cf. Daugherty and Franzini, 1965); Himmelblau and Bischoff, 1968). Using an object-oriented design philosophy, equipment objects (nodes) are those items with volume and whose state

changes occur internally, while flow streams (arcs) have no volume and serve mainly as pressure measurement points and connections between items.

For each equipment object within the network, the conservation of mass, the conservation of linear momentum and the conservation of energy can be applied to represent fluid flow and mass storage within the equipment that the node represented. Examples are pipes, wells, separators, tanks, etc.

Flow streams, however, have no volume and represent the connections between equipment nodes. It is assumed that streams have properties of mass flow rates, temperature and pressure, but no internal mass is stored within a flow stream. The continuity of flowing properties through the flow streams is assumed.

The overall network is represented computationally as an object containing a list of flow equipment items and a list of flow streams. Each equipment item is identified by an equipment type and a name, while flow streams are only identified by the equipment items that they connect.

The fundamental equations describing flow in the network (cf. Daugherty, 1965) consist of mass, momentum, and energy balance relations for each subpart of the network and continuity relationships. Since we will implement the network using detailed physical models for each equipment node, all of the balances will automatically be satisfied over every part of the network, as well as the network as a whole. In addition, a continuity constraint is needed, which is automatically satisfied by detailed internal modeling in each node and the constraint that each stream (i.e. connection between nodes) can have only a single temperature, pressure, and flow rate at any time. In other words, the outlet conditions from one equipment item must be the same as the inlet conditions for the following item. As will be seen, due to the implementation, this will be automatically ensured in the flow network model.

In order to solve the fundamental flow equations in the flow network, an iterative multi-pass algorithm has been devised. While considering flow especially through junctions where mass conservation requires a balance between the flow rates, pressures and temperatures of individual complex flow equipment items, it is apparent that the simultaneous solution of the equations of momentum, mass, and energy throughout a complex network would be difficult and likely impractical to implement. As a result, an iterated sequential solution algorithm has been devised and the following solution procedure has been implemented.

1. Sort the network equipment items in order from sources to sinks using the following procedure:
    a. Create an empty list of equipment items, then search through the network equipment and add all equipment items that do not have a defined inlet.
    b. For each equipment item in the list
        i. For each outlet stream, find the equipment associated with the outlet and add it to the list.
2. Set simulation time to zero and initialize the flow system using the following procedure:
    a. Beginning at the sources, traverse the flow network and set all rates to zero and all temperatures to a specified ambient temperature with appropriate fluid contents.
    b. Beginning at the sinks, traverse the network in a reverse direction and compute the inlet pressure for each equipment item considering static equilibrium within each equipment item.

3. Iterate through the network flow calculations until the flow rates, temperature and pressure of all flow streams do not change within a specified tolerance using the following procedure:
    a. Beginning at the sources, traverse the flow network in a forward direction and solve the applicable flow equations to determine the outlet flow rates for each equipment item in order, assuming the pressure, temperature and inlet flow rates are known.
    b. Beginning at the sinks, traverse the flow network in a reverse direction to compute the pressure at the inlet of each flow equipment item assuming that the flow rates, temperature and outlet pressures are known.
    c. Beginning at the sources, traverse the network once again in a forward direction and compute the outlet temperature for each equipment item assuming the flow rates, pressures and inlet temperature are known.
4. Print or save necessary information, advance the time step and return to step 3.

IMPLEMENTATION

The entire integrated flow model was implemented in the C# programming language using Microsoft Visual Studio™ 2008. In order to enforce the flow calculations, certain parameters and methods are required for all flow equipment and flow streams. These are implemented in the object inheritance hierarchy and the use of **override** and **virtual** methods in the C# programming language. The overall network programming

objects are defined as follows: It should be noted however, that each equipment item will add additional detail to that specified here.

In order to provide input data to IFM, an XML file format was selected because it is plain text and easily created and has enough descriptors to make it readable even to persons not trained in the use of the software. Following is a representative data file with a detailed description.

```
1. <?xml version="1.0" encoding="utf-8"?>
2. <IFM>
3. <Project Name="2 Beam Pump Wells to Tank">
4. <Environment Temperature="60" />
5. </Project>
6. <FluidSystem Type="BlackOil">
7. <Component Name="GAS" Type="Gas" GasGravity="0.7" />
8. <Component Name="OIL" Type="Oil" APIGravity="30" />
9. <Component Name="WTR" Type="Water" Salinity="0" />
10. <Phase Name="AQUEOUS" Type="Aqueous" />
11. <Phase Name="HCLIQ" Type="HCLiquid" />
12. <Phase Name="HCVAP" Type="HCVapor" />
13. </FluidSystem>
14. <Network>
15. <Equipment Type="Well" Name="W1" X="0" Y="4000" Elevation="0">
16. <Tubing ID="0.166666666666667" OD="0.19375" Roughness="0.0075"
    Length="4000" Anchor="True" />
17. <Casing ID="0.416666666666667" OD="0.4583333333333" Roughness="0.00075"
    Length="4000" Closed="False" Vent="14.7" />
18. <Completion Type="Radial" k="10.0" h="10.0" phi="0.1" S="0.0" T="110.0"
    pi="100.0" rw="0.3" re="1000.0" NR="10" WaterCut="0.0" GOR="3.0" />
19. <LiftMode Type="RodPump">
       a. <SurfaceUnit  A="30.0" C="111.07" I="48.0" P="132.0" H="213.99"
          G="45.13" R="42.0" />
       b. <Rods Type="Steel" Length="4000.0" Diameter="0.75" Segments="20"
          />
       c. <Pump Diameter="1.5" Efficiency="1.0" InitialHt="4.0" />
       d. <Operation SPM="6.0" Ttbg="60.0" />
20. </LiftMode>
21. </Equipment>
22. <Equipment Type="Well" Name="W2" X="3000" Y="-2000" Elevation="0">
23. <Tubing ID="0.166666666666667" OD="0.19375" Roughness="0.0075"
    Length="3000" Anchor="True" />
24. <Casing ID="0.416666666666667" OD="0.4583333333333" Roughness="0.00075"
    Length="3000" Closed="False" Vent="14.7" />
```

```
25. <Completion Type="Radial" k="10.0" h="10.0" phi="0.1" S="0.0" T="110.0"
    pi="100.0" rw="0.3" re="1000.0" NR="10" WaterCut="0.0" GOR="3.0" />
26. <LiftMode Type="RodPump">
       a. <SurfaceUnit  A="30.0" C="111.07" I="48.0" P="132.0" H="213.99"
          G="45.13" R="42.0" />
       b. <Rods Type="Steel" Length="3000.0" Diameter="0.75" Segments="20"
          />
       c. <Pump Diameter="1.5" Efficiency="1.0" InitialHt="4.0" />
       d. <Operation SPM="5.0" Ttbg="60.0" />
27. </LiftMode>
28. </Equipment>
29. <Equipment Type="Pipe" Name="P1" X="0" Y="4000" Elevation="0">
30. <End X="10000" Y="0" Elevation="0" />
31. <Dimensions ID="0.166666666666667" OD="0.19375" Roughness="6E-05"
    Length="10770.00" />
32. <Model Segments="54" />
33. </Equipment>
34. <Equipment Type="Pipe" Name="P2" X="3000" Y="-2000" Elevation="0">
35. <End X="10000" Y="0" Elevation="0" />
36. <Dimensions ID="0.166666666666667" OD="0.19375" Roughness="6E-05"
    Length="7280" />
37. <Model Segments="36" />
38. </Equipment>
39. <Equipment Type="Junction" Name="J1" X="0" Y="4000" Elevation="0" />
40. <Equipment Type="Junction" Name="J2" X="3000" Y="-2000" Elevation="0" />
41. <Equipment Type="Junction" Name="J3" X="10000" Y="0" Elevation="0" />
42. <Equipment Type="Pipe" Name="P3" X="10000" Y="0" Elevation="0">
43. <End X="16000" Y="0" Elevation="0" />
44. <Dimensions ID="0.166666666666667" OD="0.19375" Roughness="6E-05"
    Length="6000" />
45. <Model Segments="30" />
46. </Equipment>
47. <Equipment Type="Tank" Name="T1" X="16000" Y="0" Elevation="0">
48. <Dimensions Height="20" Diameter="8" Inlet="1" PrimaryPhase="HCLIQ" />
49. <Operation Pressure="100.0" Temperature="60" />
50. </Equipment>
51. <Stream FromEq="W1" FromName="TUBING" ToEq="J1" ToName="I1"
    BackFlow="TRUE" />
52. <Stream FromEq="W1" FromName="CASING" ToEq="J1" ToName="I2"
    BackFlow="True" />
53. <Stream FromEq="J1" FromName="O1" ToEq="P1" ToName="INLET"
    BackFlow="TRUE"/>
54. <Stream FromEq="P1" FromName="OUTLET" ToEq="J3" ToName="I1"
    BackFlow="TRUE"/>
55. <Stream FromEq="W2" FromName="TUBING" ToEq="J2" ToName="I1"
    BackFlow="TRUE" />
56. <Stream FromEq="W2" FromName="CASING" ToEq="J2" ToName="I2"
    BackFlow="True" />
57. <Stream FromEq="J2" FromName="O1" ToEq="P2" ToName="INLET"
    BackFlow="TRUE"/>
```

```
<Stream FromEq="P2" FromName="OUTLET" ToEq="J3" ToName="I2"
   BackFlow="TRUE"/>
<Stream FromEq="J3" FromName="O1" ToEq="P3" ToName="INLET"
   BackFlow="TRUE"/>
<Stream FromEq="P3" FromName="OUTLET" ToEq="T1" ToName="INLET"
   BackFlow="TRUE" />
</Network>
<Initialize>
<Equipment Name="P1" Pout="True" Pin="False" Qo="0" Qw="0" Qg="0"
   HL="1.0" FW="0.0" RS="2.0" />
<Equipment Name="P2" Pout="True" Pin="False" Qo="0" Qw="0" Qg="0"
   HL="1.0" FW="0.0" RS="2.0" />
<Equipment Name="P3" Pout="True" Pin="False" Qo="0" Qw="0" Qg="0"
   HL="1.0" FW="0.0" RS="2.0" />
</Initialize>
<SurfaceUnit1  A="56.0" C="48.17" I="48.0" P="57.50" H="106.63"
   G="45.13" R="10.0" Stroke="24" />
<SurfaceUnit2  A="30.0" C="111.07" I="48.0" P="132.0" H="213.99"
   G="45.13" R="42.0" Stroke="24" />
<SurfaceUnit3  A="129.0" C="111.07" I="111.0" P="132.0" H="232.0" G="96"
   R="42.0" Stroke="100"/>
<SurfaceUnit4  A="64.0" C="64.0" I="64.0" P="74.5" H="126.13" G="51.13"
   R="24.0" Stroke="48"/>
<SurfaceUnit5  A="64.0" C="64.0" I="64.0" P="74.5" H="126.13" G="51.13"
   R="16.0" Stroke="32"/>
</IFM>
```

Flow Network

Name:

FlowNetwork

Parameters:

Fluids – the fluid system properties to be used in the flow calculations

Equipment – a sorted list of Flow Equipment items contained in the network

Streams – a list of Flow Stream items contained in the network

Methods

None

Flow Equipment

Name:

FlowEquipment

Parameters:

`Name`– the name of the equipment item

`EquipmentType`– the type of equipment, i.e. Separator, Pipe, Well, etc.

`Location`– the x- and y-coordinates and elevation where the item is located

`Inlets`– a list of Flow Stream items representing flow inlets to the equipment item

`Outlets`– list of Flow Stream items representing flow outlets from the equipment item

Methods

`Initialize` – set the initial conditions for the equipment item

`SaveState` – save the state of the equipment item prior to a time step, must be implemented by each equipment type

`GetOutletRates` – solve flow equations internal to the equipment to determine the outlet flow rates; must be implemented by each equipment type

`GetInletPressures` – solve flow equations internal to the equipment to determine the outlet pressures; must be implemented by each equipment type

`GetOutletTemperatures` – solve flow equations internal to the equipment to determine the outlet temperatures; must be implemented by each equipment type

Flow Stream

Name:

FlowStream

Parameters:

`FromName` – the name of the FlowEquipment where the stream originates

`FromEquip` – the FlowEquipment where the stream originates

`ToName` – the name of the FlowEquipment where the stream ends

`ToEquip` – the FlowEquipment where the stream ends

`CanBackFlow` – indicates whether fluids can flow in reverse through the stream

`CurrentState` – the current state of flow rates, temperature and pressure for the stream

`SavedState` – the state of flow rates, temperature and pressure for the stream at the last time step

`LastState` – the state of flow rates, temperature and pressure for the stream at the last iteration

Methods

`Connect` – link the inlet and outlet equipment to the stream

`SaveState` – save the flow rates, temperature and pressure at the start of a time step

`SaveIterationState` – save the flow rates, temperature and pressure at the start of an iteration.

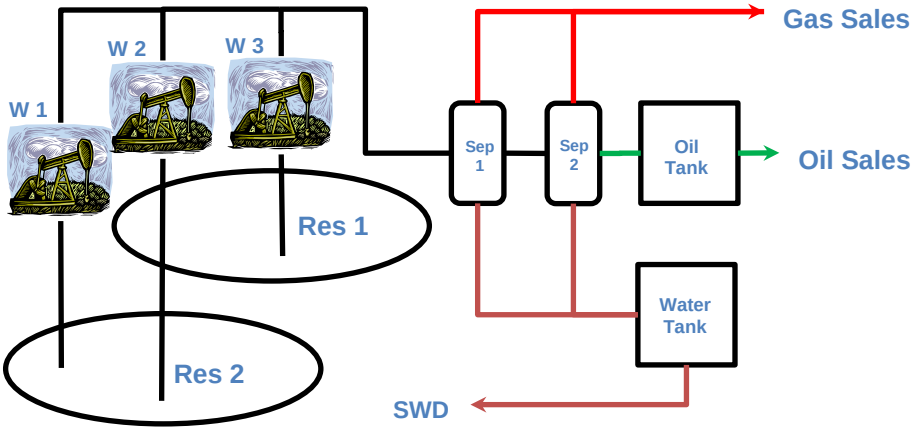

Figure 2.1. Simplified flow diagram of a typical marginal oil field.

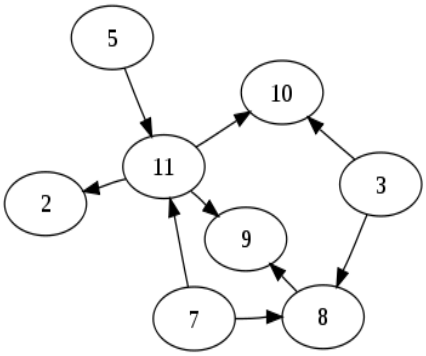

Figure 2.2. Example of a Directed Acyclic Graph (DAG, from Wikipedia).

Chapter 3: Multiphase Pipe Flow

Within the well and surface facilities, a large portion of the fluid flow occurs within pipes and piping networks. In various parts of the well and facilities, fluids may be single-phase, two-phase or three-phase; so it is necessary to develop methods to model all three situations. In addition, since a significant part of this work depends on modeling unsteady state flow, the typical assumptions of steady-state, time-invariant flow cannot necessarily be invoked. An overview of multiphase flow modeling in wellbores is presented in Brill and Mukherjee (Brill and Mukherjee, 1999) and a detailed treatment of more general multiphase flow is contained in Kolev (Kolev, 2002), (Govier and Aziz, 2008) and Shoham (Shoham, 2006).

Single-phase fluid flow has been studied extensively and finds wide application in many industries. In general, the flow is analyzed using the conservation of mass and the conservation of linear momentum as well as the conservation of energy when thermal effects are important. It is generally necessary to incorporate an empirical friction factor to account for variations in flow velocity within a pipe as well as accounting for the presence of a boundary layer in turbulent flow (Bird et al., 2007).

For multiphase, multicomponent flow, the evaluation is more complex since equations for the conservation of mass and the conservation of linear momentum of each component are required, as well as the conservation of total energy. In addition, since phase changes and interphase mass transfer may occur along the flow path, a flash procedure is needed to describe the fluid compositions at each point and an equation-of-state is required to determine the corresponding phase properties, where thermodynamic equilibrium is assumed locally.

FLOW EQUATIONS

For multiphase, multicomponent flow, a mass conservation and a momentum conservation equation are written for infinitesimal pipe segments for each component with an overall conservation of energy relation to account for thermal effects. The derivation is not presented here, but a detailed derivation is given in Shirdel (Shirdel, 2010) and in RELAP5 (RELAP5, 2012). An analysis of two-phase flow in inclined pipes was presented by Beggs and Brill (Brill and Mukherjee, 1999) for steady-state flow; however in this present work multiphase transient flow was represented following the techniques presented in the RELAP5 documentation (RELAP5, 2012) as in (RELAP5, 2012) and Shirdel (Shirdel, 2013). The fundamental equations are summarized as follows, where a black oil compositional model is assumed.

As was done by Shirdel (Shirdel, 2010), the momentum balances were taken by phase, rather than by component. Although this ignores the effect of interphase momentum transfer due to changes in the solution gas in a black oil model, the effect is small, and it was assumed that all the gas momentum is in the vapor phase. Due to the generally low mass of solution gas compared to oil, this assumption appears to be warranted. Note also that the momentum equations were simplified by expanding the terms containing velocity and substituting the mass balance equations as was done in RELAP5 (RELAP5, 2012) and Shirdel (Shirdel, 2013). Note that the momentum equations contain terms that describe drag effects for contact between the fluid and pipe wall and pipe annulus, F_{wL}, F_{aL}, F_{wG} and F_{aG}, as well as a term to describe the drag between the liquid and the gas phases, F_{LG}. These terms must be determined from multiphase flow correlations and will be described in a following section.

In modeling fluid flow in rod pumped wells, the fluid flows in the annulus between the tubing and the rods. In that case, there is drag along both the inside and the outside

diameters and additionally the inside pipe wall will likely be in motion. Calculation of the fluid drag for rods and couplings is covered in Chapter 5.

Conservation of Mass

$$\frac{\partial}{\partial t}(H_L\rho_L + H_G\rho_G) + \frac{\partial}{\partial x}(H_L\rho_L v_L + H_G\rho_G v_G) = 0 \quad \text{.....(3.1)}$$

Liquid Momentum

$$H_L\rho_L\frac{\partial v_L}{\partial t} + \frac{1}{2}H_L\rho_L\frac{\partial v_L^2}{\partial x} + 144g_c\frac{\partial}{\partial x}(H_L p) + H_L\rho_L g\,sin\theta + F_{wL} + F_{aL} - F_{LG} = 0 \quad \text{.....(3.2)}$$

Gas Momentum

$$H_G\rho_G\frac{\partial v_G}{\partial t} + \frac{1}{2}H_G\rho_G\frac{\partial v_G^2}{\partial x} + 144g_c\frac{\partial}{\partial x}(H_G p) + H_G\rho_G g\,sin\theta + F_{wG} + F_{aG} + F_{LG} = 0 \quad \text{.....(3.3)}$$

Where H_L = liquid holdup (i.e. volume fraction of liquid, fraction)

H_G = gas holdup (i.e. volume fraction of gas)

ρ_L = liquid (oil + water) density (lb/ft^3)

ρ_G = gas phase density (lb/ft^3)

g_c = gravitational constant (32.17 ft/sec^2)

θ = angle of flow above the horizontal in Rad

p = pressure (psia)

For each component, the mass balance for that component is the sum of contributions across all phases. For computational purposes, mass balance equations for oil, gas and water components, as well as oil plus gas, water plus oil, water plus gas, and total oil, water, and gas mixtures are interchangeable and any 3 of the relationships can be selected. Since the pressure calculation is mostly dependent on the total mass balance and the formulation uses total liquid (oil plus water) in the momentum relations, the equations chosen here are 1) total mass balance (oil plus water plus gas), the liquid mass balance (oil plus water) and the water mass balance. It is also assumed that the pressure and the

temperature in all phases are equal at any point along the pipe length and do not vary across the pipe diameter. The equations are:

Oil + Water Mass Balance

$$\frac{\partial}{\partial t}\left\{H_L\left[f_W\rho_W + f_O\left(\rho_O - \frac{R_S\hat{\rho}_G}{5.6146}\right)\right]\right\} + \frac{\partial}{\partial x}\left\{H_L\left[f_W\rho_W + f_O\left(\rho_O - \frac{R_S\hat{\rho}_G}{5.6146}\right)\right]v_L\right\} = 0 \quad \text{.....(3.4)}$$

Water Mass Balance

$$\frac{\partial}{\partial t}(H_L f_W \rho_L) + \frac{\partial}{\partial x}(H_L f_W \rho_L v_L) = 0 \quad \text{.....(3.5)}$$

Total Energy

$$\frac{\partial}{\partial t}\left[H_L\rho_L\left(h_L + \frac{v_L^2}{2g_cJ_c} - \frac{144\,p}{J_c\rho_L}\right) + H_G\rho_G\left(h_G + \frac{v_G^2}{2g_cJ_c} - \frac{144\,p}{J_c\rho_G}\right)\right] + (H_L\rho_L v_L + H_G\rho_G v_G)g\,sin\theta +$$
$$\frac{\partial}{\partial x}\left[H_L\rho_L\left(h_L + \frac{v_L^2}{2g_cJ_c}\right)v_L + H_G\rho_G\left(h_G + \frac{v_G^2}{2g_cJ_c}\right)v_G\right] + US(T - T_{ext}) = 0 \quad \text{.....(3.6)}$$

The energy balance is taken over all phases and incorporates an overall heat loss coefficient, U, that acts across the internal pipe perimeter, S, to describe heat lost from the fluids. Again, it is assumed that all phases, as well as the pipe material, are at the same temperature at any point along the pipe.

Annular Flow

The normal approach for modeling annular flow is to define a Reynolds number based on the annular diameter, $D_o - D_i$, then use friction factor correlations with a hydraulic diameter to estimate friction losses (Brill and Mukherjee, 1999). The approach taken in this work is to use a superposition of pipe flows to compute the equivalent drag on the annulus and the outer pipe walls as shown schematically in Figure 3.1.

To justify this approach, note that if the annulus is not in motion, the drag due to flow inside the annulus must be balanced by the friction and that the total flow rate is equal to the flow in the pipe minus the flow in the annulus. If the friction drag is properly represented by the friction factors for each flow, the force on the annulus will be equal to

the drag force due to the flow inside the annular pipe. In order to account for an annulus in motion (i.e. rods inside tubing), the velocity of the fluid relative to the annulus wall is used for calculations.

Flow Patterns

Solutions of the momentum equations for liquid and gas require evaluation of the fluid drag terms, F_{wL}, F_{aL}, F_{wG}, F_{aG} and F_{LG}. These drag terms depend highly on the flow regime and must be determined from empirical correlations. The flow patterns used in the RELAP5 documentation (RELAP5, 2012) are adopted here for both vertical and horizontal flows. Since various authors have used different flow regime names, for identification purposes, the patterns are called Stratified, Bubble, Slug, and Annular flow in this work and are shown schematically in Figures 3.2 and 3.3 for vertical and horizontal flow, respectively. The flow pattern maps for vertical and horizontal flows are shown in Figures 3.4 and 3.5, respectively.

It is important to note that the flow regime criteria presented in the RELAP5 documentation appear to represent equilibrium volume fractions and must be modified for transient flow conditions of interest in this work. This can be observed by comparing the limiting horizontal flow patterns from RELAP5 and from the Taitel and Dukler paper (Taitel and Dukler, 1976) referenced in the RELAP5 documentation. For horizontal flow, although the RELAP5 documentation indicates a transition from stratified to bubble flow as gas velocity increases at low volume fractions of gas (h_L/d approaches 1.0), the Taitel and Dukler flow patterns shown in Figure 3.5 indicate that stratified flow may not exist and the transition should be to slug (intermittent) flow. This was handled by adding a constraint to the flow pattern determination that at gas volume fractions below 0.1 (liquid holdup greater than 0.9), the default flow regime is slug flow, rather than stratified.

The flow regimes for multiphase flow is computed separately for vertical and horizontal flow. In this work, for purposes of flow pattern calculations, flow angles between 30° and 150° are considered to be vertical, while angles less than 30° from the horizontal are considered to be horizontal.

Fluid Drag

Solution of the momentum equations for liquid and gas require evaluation of the fluid drag terms, F_{wL}, F_{aL}, F_{wG} and F_{aG}, describing the drag of the liquid and gas phases on the pipe and annulus surfaces. The approach here is based on the technique presented by Chisholm (Chisholm, 1967) based on the prior work of Lockhart and Martinelli (Lockhart and Martinelli, 1949). A complete description of the constituent equations is presented in the RELAP5 software documentation (RELAP5, 2012). Essentially a two-phase pressure drop is first computed, then partitioned into pressure losses in the gas and liquid phases, and finally converted to force per unit volume terms required in the momentum equations. To model annular flow, a superposition approach was used to determine drag forces on the annulus as described above and separate force terms for pipe wall and annulus drag are independently computed using the same velocities for both pipe and annulus.

Interfacial Drag

Solution of the momentum equations for liquid and gas also require evaluation of the interfacial drag term, F_{LG} describing drag between the liquid and gas phases. In this work the approach used in the RELAP5 software (RELAP5, 2012) and by Shirdel (Shirdel, 2013) is applied, where the interfacial drag forces are computed using a drift flux model for vertical bubble and slug flow and a drag coefficient method is used for all other flow regimes.

Initial and Boundary Conditions

Solution of the momentum, mass, and energy balance equations requires both initial and boundary conditions. The initial conditions are determined by assuming static equilibrium with temperature equal to the ambient temperature. The boundary conditions for pipe flow are determined from the network definitions defined in the previous chapter, where the inlet flow rates, the outlet pressure, and the inlet temperature are determined by solving the remainder of the network.

For the inlet, the mass flux is expressed in terms of density, velocity and volume fractions and temperature is assumed known, while for the outlet, the pressure is assumed to be specified. (Note that 5.6146 ft^3/bbl, 1000 ft^3/MCF, and 86,400 sec/day are unit conversions factors.)

$$[H_L f_w \rho_w v_L]_{inlet} = \frac{5.6146\, q_w \hat{\rho}_w}{86400\, A} \quad (3.11)$$

$$\left[H_L f_o \left(\rho_O - \frac{R_S \hat{\rho}_G}{5.6146}\right) v_L\right]_{inlet} = \frac{5.6146\, q_o \hat{\rho}_o}{86400\, A} \quad (3.12)$$

$$[H_G \rho_G v_G]_{inlet} = \frac{1000\, q_g \hat{\rho}_g}{86400\, A} \quad (3.13)$$

$$T_{inlet} = T \quad (3.14)$$

$$p_{outlet} = p \quad (3.15)$$

SOLUTION OF FLOW EQUATIONS

In view of the overall network solution procedure explained in Chapter 2, it is necessary to solve the flow equations in three parts. The liquid and gas momentum equations are solved simultaneously using an iterative Newton scheme implicit in the liquid and gas velocities and assuming that the temperature, pressure and phase volume fractions are known. The pressure and phase volume fractions are next determined from the total mass balance, the liquid mass balance and the water mass balance equations in an iterative Newton scheme implicit in the pressure and phase volume fractions and assuming that the

phase velocities and temperature are known. Finally, the overall energy balance is used in an iterative Newton scheme implicit in temperature assuming that the phase velocities, pressure and phase volume fractions are known. It should be noted that although the overall solution algorithm is sequentially implicit, the network solution algorithm provides an additional iterative method to ensure that convergence of all parts of the system has been reached.

The solution of the equations is implemented by using a finite difference formulation on a staggered grid. For the momentum and energy equations, the temperature, pressure, and phase volume fractions are defined at the cell center while the phase velocities are defined at the cell boundaries as shown in Figure 3.6. For the mass balance equations, the control volume is taken with the temperature, pressure and phase volume fractions at the cell boundaries and the velocity in the center of the cell as in Figure 3.7. For all equations, an upstream weighting procedure is used to represent the values at the cell center by the values at the edges.

Momentum Balance Equations

The liquid and gas momentum equations are expressed in finite difference form as follows, where subscript *i* represents the distance coordinate and superscript *n* represents the time step level. The difference equations are implicit in velocities at the new time step and require a matrix solution technique. The implicit solution technique is generally the most numerically stable formulation and was used throughout.

$$g_{L_i} = \frac{\Delta x}{\Delta t} H_{L_i}^{\,n} \rho_{L_i}^{\,n} \left(v_{L_i}^{\,n} - v_{L_i}^{\,n-1} \right) + \frac{1}{2} H_{L_i}^{\,n} \rho_{L_i}^{\,n} \left(v_{L_i}^{\,n\,2} - v_{L_{i-1}}^{\,n\,2} \right) + 144 g_c H_{L_i}^{\,n} (p_{i+1}^{n} - p_i^{n}) + H_{L_i}^{\,n} \rho_{L_i}^{\,n} g \sin\theta \, \Delta x + \left(F_{wL_i} + F_{aL_i} - F_{LG_i} \right) \Delta x = 0 \quad \text{.....(3.16)}$$

$$g_{G_i} = \frac{\Delta x}{\Delta t} H_{G_i}^{\,n} \rho_{G_i}^{\,n} \left(v_{G_i}^{\,n} - v_{G_i}^{\,n-1}\right) + \frac{1}{2} H_{G_i}^{\,n} \rho_{G_i}^{\,n} \left(v_{G_i}^{\,n\,2} - v_{G_{i-1}}^{\,n\,2}\right) + 144 g_c H_{G_i}^{\,n} (p_{i+1}^{n} - p_i^{n}) +$$

$$H_{G_i}^{\,n} \rho_{G_i}^{\,n} g \sin\theta \, \Delta x + \left(F_{wG_i} + F_{aG_i} + F_{LG_i}\right) \Delta x = 0 \quad \text{.....(3.17)}$$

Where

ρ_L = liquid phase density (oil + water) density *(lb/ft^3)

ρ_G = gas phase density *(lb/ft^3)

g_c = gravitational constant (32.17 ft/sec2)

θ = angle of flow above the horizontal in Rad

p = pressure (psia)

These equations are solved implicitly for the phase velocities, v_L and v_G, by computing the Jacobian matrix of the derivatives of each equation with respect to the velocities at each grid point, assuming that the temperature, pressure and phase volume fractions are known. Newton iterations are then used to find the root of the equations and to determine the phase velocities. In most cases, the algorithm converges in at most two to three iterations.

Mass Balance Equations

The total mass balance equation is expressed in finite difference form as follows, where the subscript *i* represents the distance coordinate and the superscript *n* represents the time step level:

$$f_{T_i} = \frac{\Delta x}{\Delta t}\left[\left(H_{L_i}^{\,n} \rho_{L_i}^{\,n} + H_{G_i}^{\,n} \rho_{G_i}^{\,n}\right) - \left(H_{L_i}^{\,n-1} \rho_{L_i}^{\,n-1} + H_{G_i}^{\,n-1} \rho_{G_i}^{\,n-1}\right)\right] + \left(H_{L_i}^{\,n} \rho_{L_i}^{\,n} v_{L_i}^{\,n} +\right.$$

$$\left. H_{G_i}^{\,n} \rho_{G_i}^{\,n} v_{G_i}^{\,n}\right) - \left(H_{L_{i-1}}^{\,n} \rho_{L_{i-1}}^{\,n} v_{L_{i-1}}^{\,n} + H_{G_{i-1}}^{\,n} \rho_{G_{i-1}}^{\,n} v_{G_{i-1}}^{\,n}\right) = 0 \quad \text{.....(3.18)}$$

The oil/water and water mass balance equations are similarly expressed in finite difference form as follows:

$$f_{L_i} = \frac{\Delta x}{\Delta t}\left\{\left[H_{L_i}^{\,n}\left(f_{W_i}^{\,n}\rho_{w_i}^{\,n} + f_{o_i}^{\,n}\left\{\rho_{o_i}^{\,n} - \frac{R_{si}^{n}\hat{\rho}_G}{5.6146}\right\}\right)\right] - \left[H_{L_i}^{\,n-1}H_{L_i}^{\,n-1}\left(f_{W_i}^{\,n-1}\rho_{w_i}^{\,n-1} + f_{o_i}^{\,n-1}\left\{\rho_{o_i}^{\,n-1} - \frac{R_{si}^{n-1}\hat{\rho}_G}{5.6146}\right\}\right)\right]\right\} + H_{L_i}^{\,n}\left(f_{W_i}^{\,n}\rho_{w_i}^{\,n} + f_{o_i}^{\,n}\left\{\rho_{o_i}^{\,n} - \frac{R_{si}^{n}\hat{\rho}_G}{5.6146}\right\}\right)v_{L_i}^{\,n} - H_{L_{i-1}}^{\,n}\left(f_{W_{i-1}}^{\,n}\rho_{w_{i-1}}^{\,n} + f_{o_{i-1}}^{\,n}\left\{\rho_{o_{i-1}}^{\,n} - \frac{R_{si-1}^{n}\hat{\rho}_G}{5.6146}\right\}\right)v_{L_{i-1}}^{\,n} = 0 \quad (3.19)$$

$$f_{W_i} = \frac{\Delta x}{\Delta t}\left[\left(H_{L_i}^{\,n}f_{W_i}^{\,n}\rho_{W_i}^{\,n}\right) - \left(H_{L_i}^{\,n-1}f_{W_i}^{\,n-1}\rho_{L_i}^{\,n-1}\right)\right] + \left(H_{L_i}^{\,n}f_{W_i}^{\,n}\rho_{W_i}^{\,n}v_{L_i}^{\,n} - H_{L_{i-1}}^{\,n}f_{W_{i-1}}^{\,n}\rho_{W_{i-1}}^{\,n}v_{L_{i-1}}^{\,n}\right) = 0 \quad (3.20)$$

The set of three mass balance equation is solved implicitly for the pressure, p, and phase volume fractions, H_L and f_W, by computing the Jacobian matrix of the derivatives of each equation with respect to the pressure and phase volume fractions at each grid point, assuming that the phase velocities, temperature, and pressure are known. Newton iterations are then used to find the root of the equations and determine the phase velocities. In most cases the algorithm converges in two to three iterations.

Energy Balance Equation

The total energy balance equation is expressed in finite difference form as follows, where the subscript i represents the distance coordinate and the superscript n represents the time step level:

$$h_{T_i} = \frac{\Delta x}{\Delta t}\left[H_{L_i}^{\,n}\rho_{L_i}^{\,n}\left(h_{L_i}^{\,n} + \frac{v_{L_i}^{\,n^2}}{2g_cJ_c} - \frac{144p_i^n}{J_c\rho_{L_i}^{\,n}}\right) + H_{G_i}^{\,n}\rho_{G_i}^{\,n}\left(h_{G_i}^{\,n} + \frac{v_{G_i}^{\,n^2}}{2g_cJ_c} - \frac{144p_i^n}{J_c\rho_{G_i}^{\,n}}\right)\right] - \frac{\Delta x}{\Delta t}\left[H_{L_i}^{\,n-1}\rho_{L_i}^{\,n-1}\left(h_{L_i}^{\,n-1} + \frac{v_{L_i}^{\,n-1^2}}{2g_cJ_c} - \frac{144p_i^{n-1}}{J_c\rho_{L_i}^{\,n-1}}\right) + H_{G_i}^{\,n-1}\rho_{G_i}^{\,n-1}\left(h_{G_i}^{\,n-1} + \frac{v_{G_i}^{\,n-1^2}}{2g_cJ_c} - \frac{144p_i^{n-1}}{J_c\rho_{G_i}^{\,n-1}}\right)\right] + \left[H_{L_i}^{\,n}\rho_{L_i}^{\,n}\left(h_{L_i}^{\,n} + \frac{v_{L_i}^{\,n^2}}{2g_cJ_c}\right)v_{L_i}^{\,n} + H_{G_i}^{\,n}\rho_{G_i}^{\,n}\left(h_{G_i}^{\,n} + \frac{v_{G_i}^{\,n^2}}{2g_cJ_c}\right)v_{G_i}^{\,n}\right] - \left[H_{L_{i-1}}^{\,n}\rho_{L_{i-1}}^{\,n}\left(h_{L_{i-1}}^{\,n} + \frac{v_{L_{i-1}}^{\,n\ 2}}{2g_cJ_c}\right)v_{L_{i-1}}^{\,n} + H_{G_{i-1}}^{\,n}\rho_{G_{i-1}}^{\,n}\left(h_{G_{i-1}}^{\,n} + \frac{v_{G_{i-1}}^{\,n\ 2}}{2g_cJ_c}\right)v_{G_{i-1}}^{\,n}\right] + \left(H_{L_i}^{\,n}\rho_{L_i}^{\,n}v_{L_i}^{\,n} + H_{G_i}^{\,n}\rho_{G_i}^{\,n}v_{G_i}^{\,n}\right)g\sin\theta + U\,S(T_i^n - T_{ext}) = 0 \quad (3.21)$$

As in the previous cases, the equation is solved implicitly for the temperature, T, at the new time step by computing the Jacobian matrix of the derivatives of each equation with respect to the temperature at each grid point, assuming that the phase velocities, pressure, and phase volume fractions are known. Newton iterations are then used to find the root of the equations and determine the temperature. In most cases the algorithm converges in two to three iterations.

VALIDATION

In order to validate the pipe flow mathematical model, several checks were performed. The first check was the simulation of a single phase water injection well presented by (Brill and Mukherjee, 1999) in Example 2.1. Using correlations for water properties and running the simulation to steady-state conditions gave the parameters shown in Table 3.1 where the comparison to the published parameters is also shown. As can be seen, a difference of about 2.4 psi friction pressure drop over a length of 8000 ft is mainly due to a minor difference in friction factor estimation. The difference in gravity head is due to using a variable water density in IFM, rather than a constant value in the example.

Table 3.1. Comparison of IFM vs published water flow calculations.

	Mukherjee & Brill	IFM Estimate
Friction Loss (psi)	181.9	179.5
Gravity Head (psi)	3466.4	3492.4
Total Pressure Change (psi)	3284.5	3312.9

A second validation procedure used single phase transient flow corresponding to the so-called “water hammer” effect. Experimental data (Bergant et al., 2001) were

measured with water flowing in a 37.23 m pipe with an inside diameter of 22.1 mm with the far-end raised by 2.03m. A valve was closed with a closing time of 0.009 sec. The experimental pressures are shown in Figure 3.8 and the simulated results are shown in Figure 3.9. As can be seen, the timing of the pulses and the initial magnitude of the pulses are well represented but the magnitude of the pulses in Figure 3.9a do not decrease as rapidly as the experimental data. The authors attribute this to the need for a dynamic friction factor and the results simulated here correspond to the quasi-steady state friction results presented in the paper. Note however that increasing the pipe roughness from the default 0.00006 ft to 0.006 ft gives a good match to both the timing and magnitude of the pulses.

To validate the multiphase transient model in IFM, the experimental data presented by Minami (Minami, 1991; Minami and Shoham, 1994) were used. In Minami's Run 3, kerosene and air were pumped through a 1378 ft pipe 0.256 ft in diameter. After establishing a steady-state flow condition with 462 bbl/day kerosene and 200 MSCF/D air, the air injection rate was increased to 320 MSCF/D and the pressure, outlet rate and liquid holdup were recorded for about 30 minutes. The experimental data presented by Minami with simulated best-fit IFM results are shown in Figure 3.10, with additional results simulated in IFM shown in Figure 3.11.

It is important to note that to produce the results shown in Figures 3.10 and 3.11, it was necessary to force the slug flow regime in the model. Minami noted that his model correctly predicted slug flow, but his flow pattern map differs from that of Taitel and Duckler (Taitel and Dukler, 1976) in that it predicts the onset of slug flow at much lower liquid velocities. A comparison of Minami's and Taitel and Dukler's flow pattern maps for the flow dimensions used by Minami is shown in Figure 3.12. As can be seen the stable liquid and gas velocity used in the run lie on the border of the Taitel and Dukler transition to slug flow, but Minami's map clearly places the flow pattern in the slug flow region.

Since Taitel and Dukler's map has been much more widely used, no attempt was made to adjust the flow pattern determination algorithm in the IFM software, but the flow pattern was manually forced to slug flow for this prediction.

Note that the simulated results show a great similarity to the experimental data. It should be noted that the liquid holdup dropped by about 2%, the pressure at Station 1 (209 ft in the model) rose about 5 psi, and the peak pressure at Station 1 rose about 9 psi in both the model and the experiment. As a result of the comparison, it was concluded that the pipe flow algorithms are adequate for use in field-scale simulations.

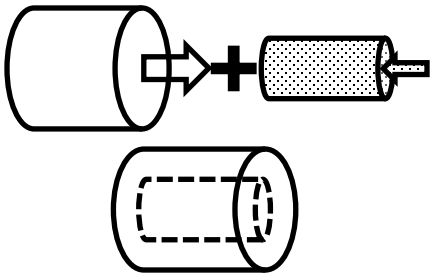

Figure 3.1. Schematic of Superposition used for Annular Flow.

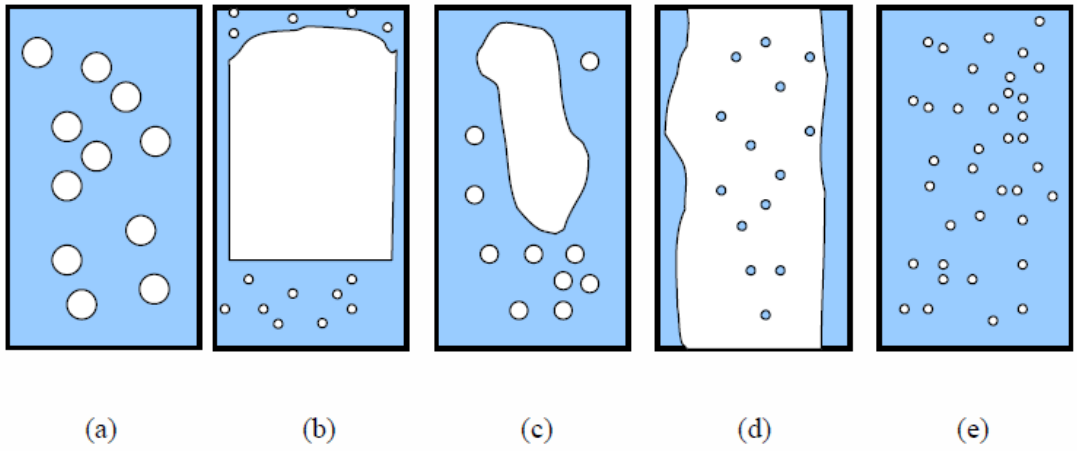

Figure 3.2. Schematic of flow regimes in vertical flow, (a) bubbly flow, (b) slug flow, (c) churn flow, (d) annular flow, (e) disperse bubbly flow (adopted from Shirdel, 2013).

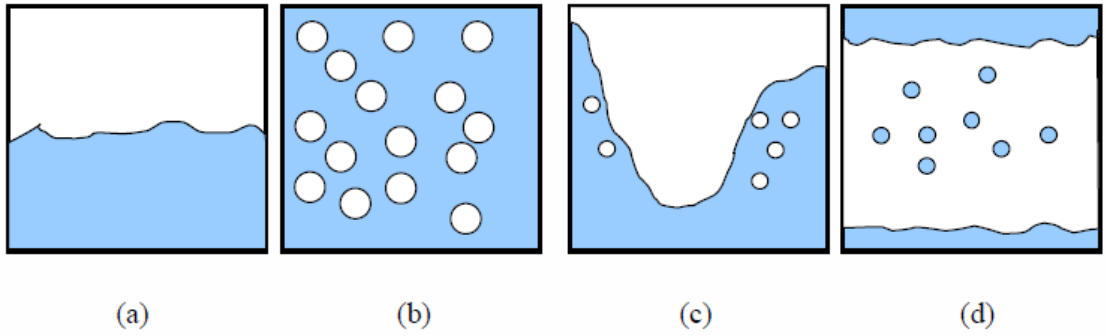

Figure 3.3. Schematic of flow regimes in horizontal flow, (a) stratified flow, (b) bubbly flow, (c) slug flow, (d) annular flow (adopted from Shirdel, 2013).

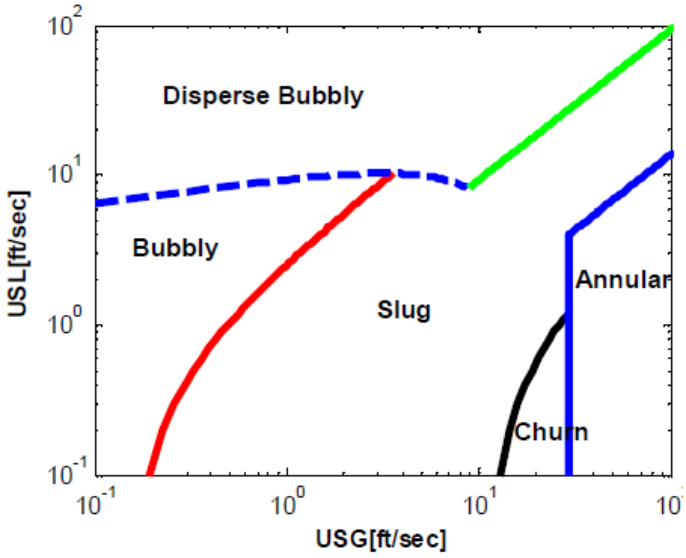

Figure 3.4. Flow pattern map for vertical flow (adopted from Shirdel, 2013).

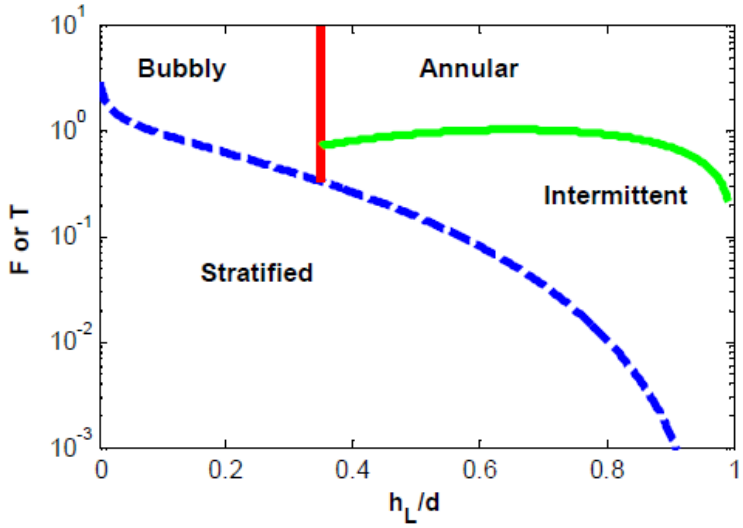

Figure 3.5. Flow pattern map for horizontal flow (adopted from Shirdel, 2013).

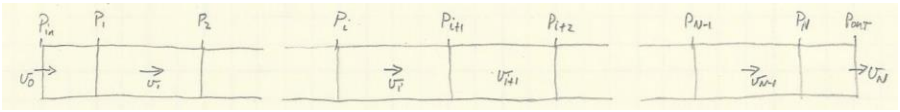

Figure 3.6. Schematic of grid used in solution of momentum and energy equations.

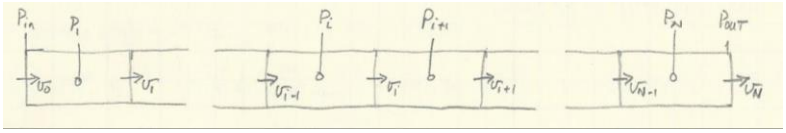

Figure 3.7. Schematic of grid used in solution of mass equations.

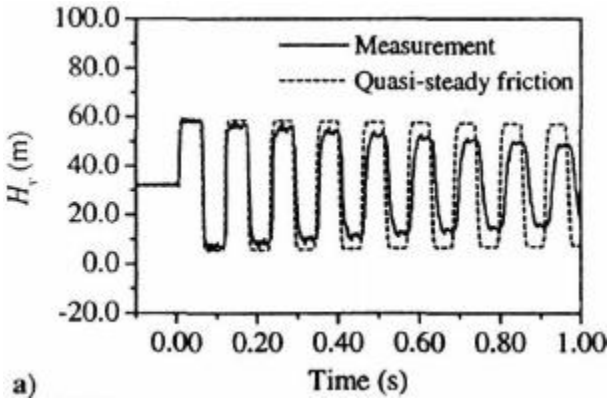

Figure 3.8. Water hammer experimental data from Bergant et al. (2001), Figure 2.

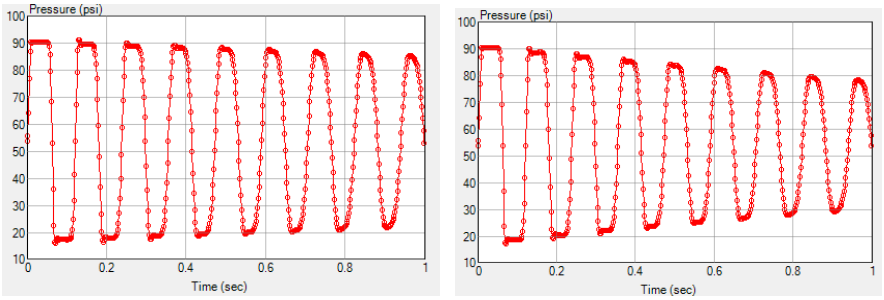

a b

Figure 3.9. Water hammer predictions (a) Roughness = 0.00006 ft, (b) Roughness = 0.006 ft.

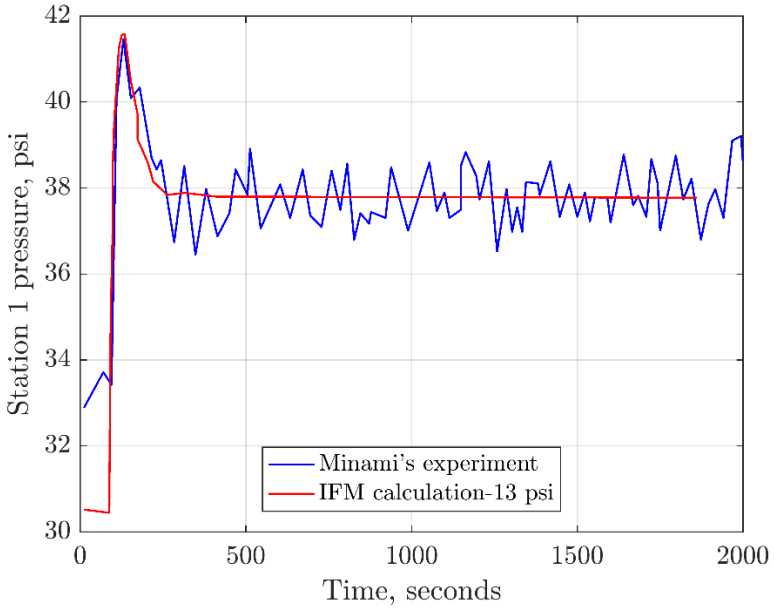

Figure 3.10. Multiphase experimental data Run 3 from Minami's dissertation with best-fit IFM calculation (Minami, 1991).

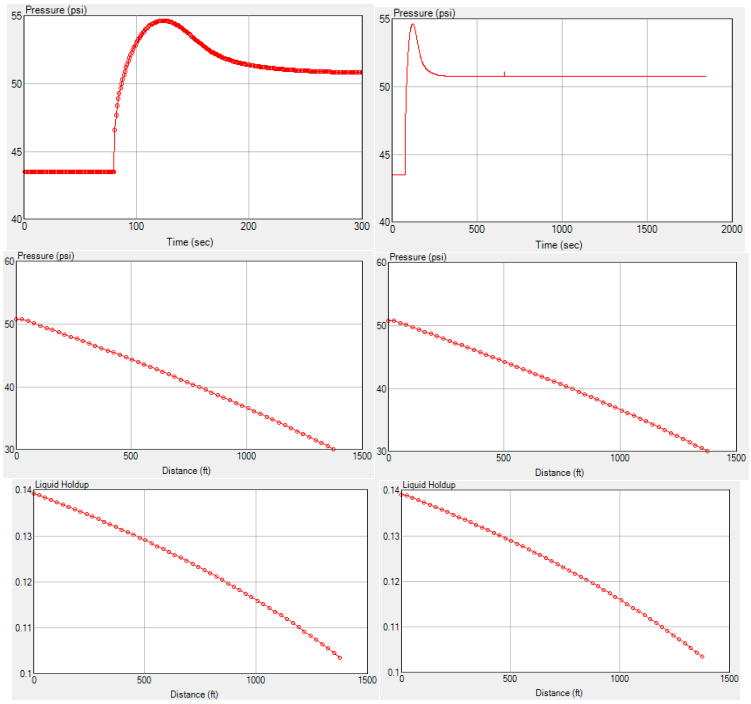

Figure 3.11. Simulated Minami Run 3 (Minami, 1991).

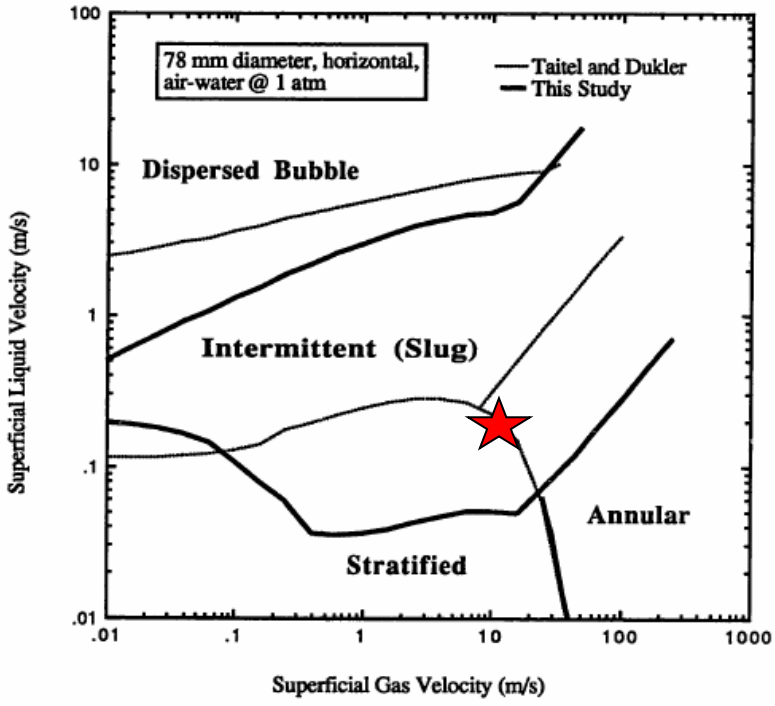

Figure 3.12. Comparison of Minami (Minami, 1991) and Taitel & Dukler (Taitel and Dukler, 1976) flow regime maps.

Chapter 4: Multiphase Separators

Within the surface facilities, fluid separation plays an important role in producing saleable oil, ensuring that the disposal water does not contain significant amounts of oil and that water does not carry over into the gas sales line. Separation systems also determine to some extent the quality of sales oil and gas. As such, it is important to be able to model separators in order to optimize the production and the value of production from wells, as well as the quality of the water that will be disposed of or re-injected. In the industry a variety of separators are used, ranging from vertical and horizontal separators relying on gravity to segregate the fluids, to vortex separators that use centrifugal forces to accelerate the separation process. Separators may also contain coalescing plates and other mechanisms that cause droplets to coalesce more rapidly.

An overview of separator characteristics and operation is provided by Langston (2003) and separator design is explained by Arnold and M. Stewart (1999). Separator design is usually based on consideration of worse case scenarios wherein the residence time is selected to ensure that droplets of a certain size are able to rise or fall and coalesce before fluids exit the separator. While this is sufficient for separator design and sizing, it provides little insight into the dynamic behavior of a separator, nor does it allow quantifying the effect of exceeding the separator design capacity.

Several authors have presented detailed models of separators based on Computational Fluid Dynamics (CFD) and the dynamics of droplet size distributions. Examples of these modeling efforts have been presented in the literature. See Frankiewicz and Lee (2002); Hafskjols et al. (1999); Hallinger et al. (1996); Song et al. (2010). In general these models appear to be computationally intensive and not directly suitable for

inclusion in an integrated model that also includes many other computationally intensive modules.

For that reason, a simplified model of gravity separators was developed for use in the integrated field model. Since gravity separators are the most common type of separator used in marginal field applications, work was focused on modeling the operation of vertical gravity separators using basic physics to honor the gravitational segregation process and obtain a dynamic model of separator performance. In the case of gravity segregation, the process is based on the application of Stokes' Law, Bird et al. (2007), for drop motion.

VERTICAL SEPARATOR

The most common separator used in marginal oil fields is probably a vertical gravity separator known as "wash tank" or "gun barrel." It consists of a gas separation unit at the inlet that allows gas to flow directly to the gas handling system and a large vertical tank where oil and water separate due to gravity. The oil and water enter the separator through an inlet pipe usually terminated in a serrated plate that forces the oil and water mixture to spread out across the tank's cross section. An oil outlet is located well above the inlet and a water outlet is located near the base of the separator. A schematic diagram of a vertical separator is shown in Figure 4.1. Due to the density difference between gas and liquids, gas separation is not usually a concern; so the effort in this work has focused on modeling the separation of oil and water.

Fundamental Equations

The fundamental relation that describes gravity segregation is Stokes' Law, which describes the terminal velocity of a spherical drop that rises or falls through a liquid of a different density. For the purposes of separator modeling, Stokes' Law can be stated as Equation 4.1 (Arnold, 1999), where $\Delta\rho$ is the density difference between the fluids (lb/ft^3),

d is the droplet diameter (micron), and μ is the viscosity of the continuous phase (cp). Velocity can increase due to large density differences, large drop sizes and lower viscosity of the continuous phase.

$$v_t = \frac{1.11x10^{-6}\Delta\rho d^2}{\mu} \quad (4.1)$$

To model a vertical separator an approach similar to that presented by Rosso and Sona (2001) is taken. Rosso and Sona considered simplified volume fraction distributions and attempted to solve the resulting equations analytically, but for the purpose of general separator modeling a more flexible and general approach is needed, whereby the volume fraction distributions are general and sources and sinks must be considered to represent the inflow and outflow of fluids from the separator.

For detailed modeling, it is assumed that the velocity in the separator is low enough that transient velocity effects can be neglected. Under that assumption, it is apparent that the inlet flow must divide between the oil outlet and the water outlet. In the ideal case, it can be assumed that the downward volumetric flow toward the water outlet is equal to the volumetric inflow of water and, conversely, the upward volumetric flow of fluids toward the oil outlet is equal to the volumetric inflow of oil. This is expressed in the following equations, where subscript *s* represents standard conditions.

$$v_{T+} = \frac{q_{so}}{A}\frac{\rho_{so}}{\rho_o} \text{ and } v_{T-} = \frac{q_{sw}}{A}\frac{\rho_{sw}}{\rho_w} \quad (4.2)$$

Normally water would flow downward relative to oil due to gravity. Using the oil velocity as a reference, the water velocity can be expressed as the oil velocity less the water relative velocity determined from Stokes' law. To maintain a volumetric balance, the total velocity can also be expressed in terms of oil and water velocities as follows.

$$v_w = v_o - \Delta v \quad (4.3)$$

$$v_T = (1 - f_w)v_o + f_w v_w \quad (4.4)$$

Substituting and rearranging yields an expression for the oil and water velocities in terms of the total velocity and the relative velocity difference.

$$v_o = v_T + f_w \Delta v \quad (4.5)$$

$$v_o = v_T - (1 - f_w)\Delta v \quad (4.6)$$

During operation of the separator, a constant operating pressure is assumed to be maintained above the liquid. For steady state, that implies a constant gas volume and therefore, if the gas separation is assumed to be perfect, the gas inflow will be equal to the gas outflow.

To compute the pressure distribution within the separator, the total liquid density is integrated from the liquid level downward. This is expressed as Equation 4.7.

$$p(z) = p_{gas} + \int_z^{z_{gas}} [(1 - f_w)\rho_o + f_w \rho_w] dz \quad (4.7)$$

Finally, it is also necessary to compute the changes in the distribution of the volume fraction of fluids based on a mass balance of one of the phases. Choosing water to be consistent with the balance equations used in pipe flow, the mass balance equation can be written as:

$$\frac{\partial}{\partial t}(f_w \rho_w) + \frac{\partial}{\partial z}(f_w \rho_w v_w) - \frac{q_{sw}\rho_{sw}}{A\,\Delta z} = 0 \quad (4.8)$$

where q_{sw} represents a source of fluids entering the separator per unit height. Normally this term will be zero, except at the inlet and the outlet to the separator. It should also be noted that inlet flow rates are positive, while outlet flow rates will be negative in this formulation.

Temperature in the separator is evaluated using an energy balance equation similar to Equation 3.10 for pipe flow. Since the velocity within the separator is generally very low and dominated by gravity, the pressure gradient and gravity terms cancel and the kinetic energy term is assumed to be insignificant. In terms of internal energy, e, the energy balance can be written as:

$$\frac{\partial}{\partial t}(f_w\rho_w e_w + f_o\rho_o e_o) + \frac{\partial}{\partial z}(f_w\rho_w e_w v_w + f_o\rho_o e_o v_o) - \frac{q_{sw}\rho_{sw}e_{sw}+q_{so}\rho_{so}e_{so}}{A\,\Delta z} + US(T - T_{ext}) = 0 \quad \text{.....(4.9)}$$

The energy relation can be simplified by expanding the partial derivatives, substituting the mass balance equations for both oil and water and expressing the derivatives of the internal energy as heat capacity multiplied by temperature derivatives. In this form, the equation becomes:

$$\left(f_w\rho_w c_{pw} + f_o\rho_o c_{po}\right)\frac{\partial T}{\partial t} + \left(f_w\rho_w c_{pw} v_w + f_o\rho_o c_{po} v_o\right)\frac{\partial T}{\partial z} - \frac{q_{sw}\rho_{sw}c_{psw}+q_{so}\rho_{so}c_{pso}}{A\,\Delta z}(T - T_s) + US(T - T_{ext}) = 0 \quad \text{.....(4.10)}$$

Numerical Solution

Solutions of the equations representing separator behavior are straightforward, except for the determination of the relative phase velocity from Stokes' law and the determination of the water volume fraction from the mass balance equation, which will be discussed in more detail.

At each time step the total velocity above and below the inlet height is calculated with equation 4.2, and then Equations 4.5 and 4.6 are used directly to compute the velocity of oil and water phases, respectively.

The volume fraction of water in each vertical cell is computed from the mass balance for water in Equation 4.8 using an implicit formulation and weighting based on the direction of volume fraction change. Since the formulation is nonlinear, the following difference equation is used and a Newton iteration is performed by evaluating the Jacobian. Note that the terms in braces depend on the direction of the weighting.

$$g_i = f_{wi}^n \rho_{wi}^n - f_{wi}^{n-1} \rho_{wi}^{n-1} + \frac{\Delta t}{\Delta z} \begin{Bmatrix} f_{wi}^n \rho_{wi}^n \\ \text{or} \\ f_{wi+1}^n \rho_{wi+1}^n \end{Bmatrix} v_{wi}^n - \frac{\Delta t}{\Delta z} \begin{Bmatrix} f_{wi-1}^n \rho_{wi-1}^n \\ \text{or} \\ f_{wi}^n \rho_{wi}^n \end{Bmatrix} v_{wi-1}^n$$

$$- \frac{q_{sw}\rho_{sw}}{A} \frac{\Delta t}{\Delta z} = 0 \quad \text{.....(4.11)}$$

where the exponent, *n*, represents the time step.

When the volume fraction of water has been determined, the updated pressure distribution in the separator is evaluated with Equation 4.7 using the trapezoidal rule and the phase densities are updated.

Finally, a heat balance is performed to determine the temperature distribution using the energy equation in the form of Equation 4.10. As for the mass balance, an implicit finite difference scheme is used and the Jacobian is computed for an iterative solution. The finite difference once again depends on weighting and is expressed as follows:

$$h_i = \rho_{Li}^n c_{pLi}^n (T_i^n - T_i^{n-1}) + \frac{\Delta t}{\Delta z} \rho_{Li}^n c_{pLi}^n v_{Li}^n \begin{Bmatrix} T_i^n - T_{i-1}^n \\ \text{or} \\ T_{i+1}^n - T_i^n \end{Bmatrix}$$

$$- \frac{q_{sL}\rho_{sL}c_{psL}}{A} \frac{\Delta t}{\Delta z} (T_i^n - T_{si}^n) + \pi DU (T_i^n - T_{ext}^n) = 0 \quad \text{.....(4.12)}$$

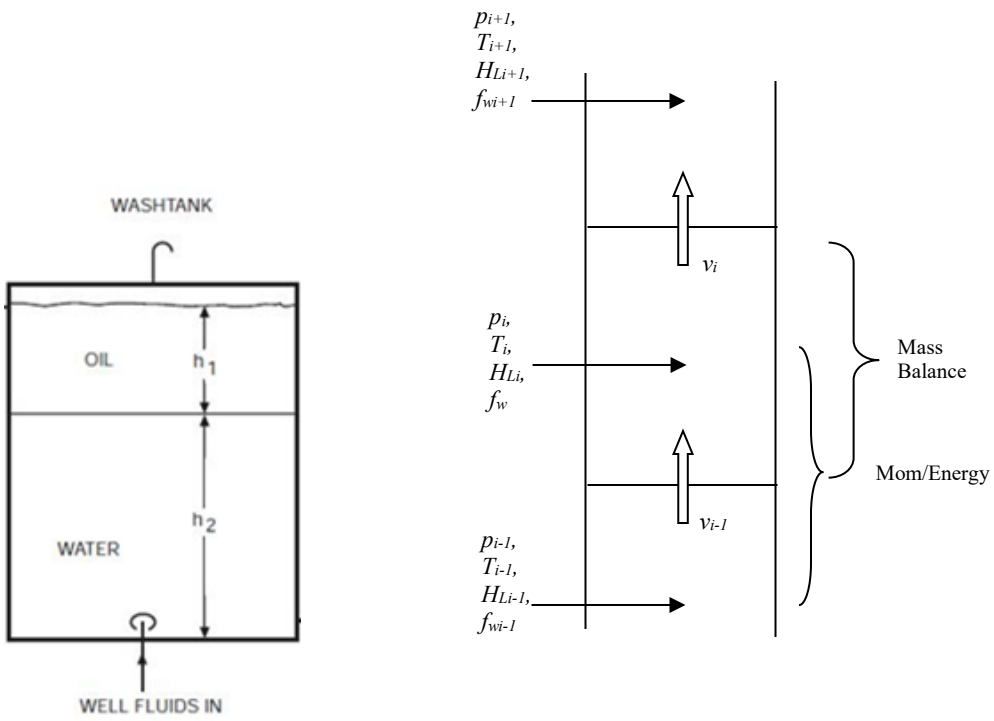

Figure 4.1. Schematic of a typical vertical separator.

Chapter 5: Well Model

It seems obvious that nearly all fluids flowing in an oil field come from wells, so representing well performance is an important part of the overall field modeling. In order to model well performance, it is also necessary to consider the inflow of fluids from the reservoir and the detailed wellbore dynamics accounting for artificial lift methods. For the purpose of the full field model documented in this work, two cases are considered. In the first case, for testing purposes, a constant rate well is modeled, while for more practical situations, the case of a beam pumped well typically used in marginal oil fields is modeled.

CONSTANT RATE WELL

In order to test the software, it is convenient to have a constant rate source. While the equation for a constant rate source is simple, when considering transient flow, large magnitude transient pressures arise during the simulation. These transients are analogous to the well-known "water hammer" phenomenon; for example, as measured by Bergant et al. (2001). In order to more realistically represent field conditions of valves opening in a finite time, a valve time parameter, Δt_v, is defined and the flow rises in a sinusoidal manner over the length of the valve opening time. In the software, a default value of 1 second is applied. The resulting equation for the rate is shown in Equation 5.1 and the rate is shown in Figure 5.1.

$$q_j = \begin{cases} \frac{q_{j\,input}}{2}\left[1 + \sin\left(\frac{\pi t}{\Delta t_v} - \frac{\pi}{2}\right)\right] & t < \Delta t_v \\ q_{j\,input} & t \geq \Delta t_v \end{cases} \quad \text{.....(5.1)}$$

BEAM PUMPS

Rod pumps are normally modeled using the damped wave equation, which is derived by applying Newton's equation for motion to infinitesimal segments of the rods and considering forces due to stress in the rods and drag forces due to fluid drag and assuming that rod stretch is represented by using a Young's modulus to relate stress and strain in the rods. Early analyses of rod pump behavior used trial and error approaches, and then analog computers were used to solve the resulting wave equations. A more complete history and literature review of historical rod pump modeling has previously been presented by several authors (cf. Lekia and Evans, 1995), but most of the recent models can be traced back to Gibbs (1963), where a numerical solution to the damped wave equation was presented. Methods for solving the equations presented by Gibbs are presented by several authors (cf. Gibbs and Neely, 1966; Schafer and Jennings, 1987); however, use of the Gibbs formulation requires estimation of the empirical damping factor which may be difficult. In fact some authors (cf. Schafer, 1987) suggest that different damping factors should be used on the upstroke and downstroke calculations.

Various authors have extended the Gibbs model. Csaszar et al. (1991) added the effect of fluid inertia to the basic model and showed that it may affect the results under some conditions. Doty and Schmidt (1983) added fluid drag to the rod motion equations by using friction factor correlations from Valeev and Repin (1976) to represent the drag effects and reported the effects of both fluid inertia and rod and coupling drag on the calculated rod loads. Lekia (1995) followed a similar procedure to account for rod drag using fluid flow models with an additional drag force due to rod couplings represented by the Valeev and Repin (1976) friction factors, but his multiphase model assumed homogeneous, no-slip, bubble flow. Later Barreto Filho (2001) accounted for a variable fluid level on the downhole pump and used the Valeev (1976) friction factors for rod

coupling drag, but assumed single phase laminar flow in the rod and tubing annulus. Xu et al. (1999) later extended the rod pump model to incorporate Coulomb friction due to the rods rubbing on the tubing due to well deviation, and also coupled multiphase flow through the use of friction factors determined using computational fluid dynamics.

Besides the rod drag and the fluid formulation, very little other works appears to have been done on representing the boundary conditions required for solution of the equations of motion. Most rod pump models have assumed constant tubing pressure (cf. Lekia, 1995) or pump plunger load and have ignored transient reservoir flow effects. A steady-state reservoir inflow model was used by Barreto Filho (2001) to account for variations in fluid level and pump intake pressure, but most other authors have ignored the effect of reservoir transients and coupling of the tubing to a surface flow system. Figure 5.2 shows pressure fluctuations measured at the tubing on a beam pumping well by Pennebaker (2014). Although the pressure scale is calibrated in analog-digital converter voltage, the scale is linear and indicates a fluctuation from a low of about 50 psi and peaks of about 150 psi. Since the stroke rate was reported to be 6 SPM, it is apparent that there are two peaks during each rod cycle. Personal experience also indicates that tubing pressure fluctuations are commonly observed on rod pump wells, although they are rarely reported due to gauge inertia and not recorded at a high enough sampling frequency.

As a result of these considerations, a more complex rod pump modeling system has been developed which removes the empirical damping factor from the rod drag calculations, couples fluid friction and rod drag forces, represents transient flow throughout the system, and couples the rod pump model to a transient flow reservoir model. Since this system allows the evaluation of the various effects that have been neglected in previous models, it can be used to determine when it is valid to ignore the neglected effects, and also

allows the evaluation of new diagnostics and analytical procedures that make use of the transient system behavior.

Rod Motion

In this work a generalized force and momentum balance on the rod string is used to determine the equation of motion describing the rod behavior. This is the same approach used by both Lekia (1995) and Barreto Filho (2001). The partial differential equation for rod motion is shown in Equation 5.2.

$$\frac{\partial^2 u}{\partial t^2} = \frac{E_r}{\rho_r}\frac{\partial^2 u}{\partial x^2} + g - (F_{aL} + F_{aG}) + \frac{P}{\rho_r A_r}\frac{dA_r}{dx} \quad \text{.....(5.2)}$$

where

u = rod velocity (ft/sec)

x = distance (ft)

E_r = Young's modulus for rod material (psi)

A_r = Cross sectional area of rods (ft^2)

g = acceleration due to gravity (ft/sec/sec)

F_{aL} drag force on rods due to liquid (lbf/ft)

F_{aG} drag force on rods due to gas (lbf/ft)

P = pressure (psia)

x = distance along unstressed rods (ft)

ρ_r = density of rod material (lb/ft^3)

Gibbs (1963) used an empirical damping factor to account for drag forces, where the drag force is proportional to the rod velocity. In this work we use a friction factor formulation for flow in pipes to couple the fluid friction to the drag forces on the rods; thus the rod drag forces per unit length are described by the F_{aL} and F_{aG} terms in the pipe flow momentum equations documented in Chapter 3. This approach ensures consistency in the

pressure drop due to flow with the corresponding rod drag forces; it has previously been presented by Lekia (1995) for single phase and multiphase flow and by Barreto Filho (2001) for single phase laminar flow.

At first thought, it would appear that the normal pipe friction terms could be used to describe drag on the rods in the tubing rod annulus. However, it is important to note that the pipe friction relations based on Reynolds number and roughness also assume uniform flow along the length of the pipe, but in the rod tubing annulus the flow is not uniform due to restrictions caused by the rod couplings. Friction factors for flow in the rod-tubing and coupling-tubing annulus were presented by Valeev and Repin (1976) and used by both Lekia (1995) and by Barreto Filho (2001) in their models. In this work we also use the Valeev and Repin friction factors and apply them in a manner equivalent to that of Barreto Filho, whereby the tubing and rod friction loss is modified by a factor depending on the additional losses imposed by the rod couplings. The following relations are used for liquid flow and the analogous relation is used for gas. The effect of any rod centralizers is ignored.

$$F'_{aL} = F_{aL} D_t \left[1 + \frac{52000\left(\frac{D_c}{D_t} - 0.381\right)^{2.57} \left\{ 2.77 \pm 1.69 \frac{R'_{eL}}{R_{eL}} \right\}}{\frac{96}{R_{eL}} \left[1 \pm \frac{R'_e}{R_e} \left(0.2 + 0.39 \frac{D_r}{D_t} \right) \right]} \right] \quad \text{.....(5.3)}$$

$$R_{eL} = \frac{\rho_L v_L (D_t - D_r)}{\mu_L} \ , \ R'_{eL} = \frac{\rho_L v_r (D_t - D_r)}{\mu_L} \quad \text{.....(5.4)}$$

where

ρ_L = density of liquid (lb/ ft^3)

μ_L = viscosity of liquid (cp)

D_t = tubing diameter (ft)

D_c = coupling diameter (ft)

D_r = rod diameter (ft)

F_{aL} = drag force on rods due to liquid (lbf/ft)

F_{aG} = drag force on rods due to gas (lbf/ft)

R_{El} = Reynolds number for liquid flow

$$F'_{aG} = F_{aG} D_t \left[1 + \frac{52000\left(\frac{D_c}{D_t} - 0.381\right)^{2.57} \left\{ 2.77 \pm 1.69 \frac{R'_{eG}}{R_{eG}} \right\}}{\frac{96}{R_{eG}} \left[1 \pm \frac{R'_{eG}}{R_{eG}} \left(0.2 + 0.39 \frac{D_r}{D_t} \right) \right]} \right] \quad \text{.....(5.5)}$$

$$R_{eG} = \frac{\rho_G v_G (D_t - D_r)}{\mu_G} \ , \ R'_{eG} = \frac{\rho_G v_r (D_t - D_r)}{\mu_G} \quad \text{.....(5.6)}$$

Given the fundamental rod motion equation, the equation is converted to finite difference form for numerical solution. The methods used by Gibbs (1963) and by Everitt and Jennings (1992) are modified in this work to derive an explicit rod motion calculation whereby the time step is not assumed to be constant. Since two time levels are required to approximate the second derivative with respect to time, this allows automatic time step adjustments while the model is running. The resulting explicit finite difference equation is as follows.

$$\begin{aligned} u_i^{n+1} = [& (A_{ri+1} u_{i+1}^n - 2A_{ri} u_i^n + A_{ri-1} u_{i-1}^n) \frac{a^2 \Delta t_n (\Delta t_n + \Delta t_{n-1})}{2\Delta x^2} \\ & + \frac{(\Delta t_n + \Delta t_{n-1})}{\Delta t_{n-1}} A_{ri} u_i^n - \frac{\Delta t_n}{\Delta t_{n-1}} A_{ri} u_i^{n-1} \\ & - \frac{A_t}{\rho_r g_c A_{ri}} (F_{aLi} + F_{aGi}) \frac{\Delta t_n (\Delta t_n + \Delta t_{n-1})}{2}] / A_{ri} \end{aligned} \quad \text{..... (5.7)}$$

where

u = rod velocity (ft/sec)

A_r = rod cross sectional area (ft^2)

Initial and boundary conditions are also required for the solution of the rod string motion. The initial condition is computed by assuming the rods are hanging in static equilibrium with the stress and the corresponding strain computed from the buoyant rod weight at each point in the rod string. The boundary conditions consist of the polish rod position at each time step, *u[0,t]*, as well as the load at the pump computed from the tubing flow and downhole pump pressure relations described below.

Surface Pumping Unit

In this study the Gray (1963) pumping unit model is used whereby the motion is represented by a 4 bar problem with the driven element (R in Figure 5.1) rotating at a constant rate.. Standard API unit dimensions are used throughout, and a constant angular velocity of element R in Figure 5.1 is assumed. Future work should incorporate motor slippage but is not considered here. Using API pumping unit geometry nomenclature, the relations are as follows:

$$L_2 = \sqrt{(H-G)^2 + I^2} \quad (5.8)$$

$$C_1 = \cos(\theta + \theta_c) \quad (5.9)$$

$$C_2 = \sqrt{1 + \left(\frac{R}{L_2}\right)^2 + 2C_1\frac{R}{L_2}} \quad (5.10)$$

$$C_3 = \frac{1}{C_2}\left(a_a + \frac{RC_1}{C}\right) \quad (5.11)$$

$$C_4 = \frac{R\sin(\theta+\theta_c)}{C_2 L_2} \quad (5.12)$$

$$a_a = \frac{R^2+L_2^2+C^2-P^2}{2L_2C} \quad (5.13)$$

$$\alpha = \tan^{-1}\left(\frac{C_4}{\sqrt{1-C_4^2}}\right) \quad (5.14)$$

$$\beta = \cos^{-1}(C_3) \quad (5.15)$$

$$x_0 = \frac{1}{12}[A(\alpha+\beta) - x_{min}] \quad (5.16)$$

$$\theta^n = \theta^{n-1} + \frac{2\pi\Delta t_n}{60/SPM} \quad (5.17)$$

The surface polish rod position is advanced by assuming a constant angular velocity, whereby 2π radians are traversed during each stroke. The surface position shown as x_0 in Equation 5.16 is the surface position of the rod string at the new time step, $u[0,t_n]$.

Downhole Pump

The downhole pump is modeled using a simple mass balance to determine pump pressure. Variation of pressure with position inside the pump and plunger inertia are not considered; complete separation of gas before entry into the pump is not assumed in the models presented here. The internal pump volume depends on the plunger position which is equal to the bottom of the rod string. Since the fluid properties depend on pressure, the pump pressure is determined by searching for the root of Equation 5.18.

$$V_p^n = V_p^{n-1} + (u_L^n - u_L^{n-1}) = V_o^n B_o + V_w^n B_w + \left(V_g^n - R_s V_o^n\right) \quad \text{.....(5.18)}$$

Once the internal pump pressure is known, the load on the plunger can be computed by the pressure difference between the tubing pressure above the pump and the internal pump pressure, multiplied by the net plunger area. This serves as a load boundary condition on the bottom of the rod string, whose equation of motion was previously described.

$$\frac{\partial u_L^n}{\partial x} = \frac{A_p(p_{tN}^n - p_p^n)}{E_r A_p} \quad \text{.....(5.19)}$$

In addition, the pump plunger motion provides a boundary condition for mass flow into the bottom of the tubing. During the upstroke the plunger moves upward and the volumetric flow into the bottom of the tubing is equal to the area of the pump-rod annulus times the plunger velocity, and the volumetric flow into the pump from the wellbore is equal to the plunger area times the plunger velocity. Similarly, during the down stroke, the rods displace fluids inside the pump barrel, so the volumetric flow into the base of the tubing is equal to the rod area times the plunger velocity. During the stroke, the traveling and standing valves states (open or closed) are determined based on the pressure difference between the internal pump and the tubing pressure or the external wellbore pressure.

CASING ANNULUS

In the casing, it is assumed that there is no net liquid flow inside the casing tubing annulus and that gas is bubbling through a static liquid column. The correlation presented by Gilbert (1954) is used to determine the liquid and gas volume fraction in the gaseous liquid column. The fluid mass inside the casing is computed from the reservoir flow equation and a superficial gas velocity is thereby determined. Above the perforations, there is a gaseous liquid column with a liquid holdup determined from Gilbert's correlation (Gilbert, 1954) using the superficial gas velocity. Above the gaseous liquid column, free gas is assumed to go to the surface. The volume of oil water and gas is computed from mass balance and if constant surface casing pressure is specified, the volume of gas to the fluid level is computed, so that the bottom hole pressure of the fluid column is equal to the reservoir pressure. If a closed annulus is specified, the surface pressure is found by searching for the root of the volume balance using pressure dependent fluid properties.

Fluid from the gaseous liquid column flows into the pump based on the plunger velocity and pump area, and the volumetric flow into the pump from the casing annulus, therefore both liquid and free gas may enter the pump. Similarly, during the down stroke, the rods displace fluids inside the pump barrel, so the volumetric flow into the base of the tubing is equal to the rod area times the plunger velocity. During the stroke, the traveling and standing valves states (open or closed) are determined based on the pressure difference between the internal pump and the tubing pressure or the external wellbore pressure.

When the traveling valve is open on the downstroke, it is assumed that free gas inside the pump will enter the tubing first and liquids will enter only when all the free gas has been depleted from the pump. It is important to note that in most of the cases presented later in this dissertation, no free gas is found in the pump since the pressure is generally above the bubble point pressure and all gas is in solution.

RESERVOIR AND COMPLETION MODEL

To represent transient fluid flow from the reservoir into the wellbore a radial flow reservoir model similar to that used in pressure transient analysis is used as presented by Earlougher (1977) among others. The reservoir model includes skin at the wellbore and relates the fluid flow into the well to the pressure distribution in the near well area.

$$\frac{1}{r}\frac{\partial}{\partial r}\left(r\frac{\partial p}{\partial r}\right) = \frac{0.000264k}{\varphi\mu c_t r_w^2}\frac{\partial p}{\partial t} \quad (5.20)$$

$$p_w = p_{r_w} - \frac{kh}{141.2B_o\mu}S\left(r\frac{\partial p}{\partial r}\right)_{r=r_w} \quad (5.21)$$

$$q_o = \frac{kh}{141.2B_o\mu}\left(r\frac{\partial p}{\partial r}\right)_{r=r_w} \quad (5.22)$$

$$q_g = Rq_o \quad (5.23)$$

$$q_w = \frac{fw}{1-fw}q_o \quad (5.24)$$

$$q_{ot}^n = \begin{cases} (1-f_w)\frac{dV_p}{dt}B_o & \left(V_g^n - R_sV_o^n\right) \le 0 \\ 0 & \left(V_g^n - R_sV_o^n\right) > 0 \end{cases} \quad (5.25)$$

$$q_{wt}^n = \begin{cases} f_w\frac{dV_p}{dt}B_w & \left(V_g^n - R_sV_o^n\right) \le 0 \\ 0 & \left(V_g^n - R_sV_o^n\right) > 0 \end{cases} \quad (5.26)$$

$$q_{gt}^n = \begin{cases} \frac{dV_p}{dt}B_g & \left(V_g^n - R_sV_o^n\right) > 0 \\ 0 & \left(V_g^n - R_sV_o^n\right) \le 0 \end{cases} \quad (5.27)$$

In contrast to normal pressure transient testing, a pressure boundary condition is applied at the wellbore, whereby the flow into the well is controlled by the pressure inside the wellbore. Since the pressure varies with pump action and annular fluid level, a constant or steady state flow rate will never be reached in general.

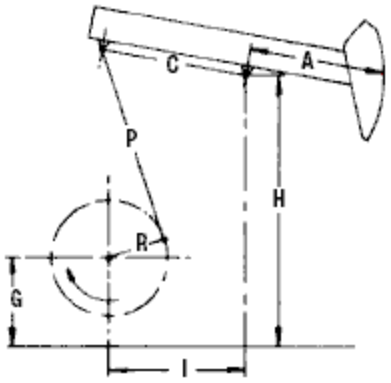

Figure 5.1. API pumping unit geometry parameters.

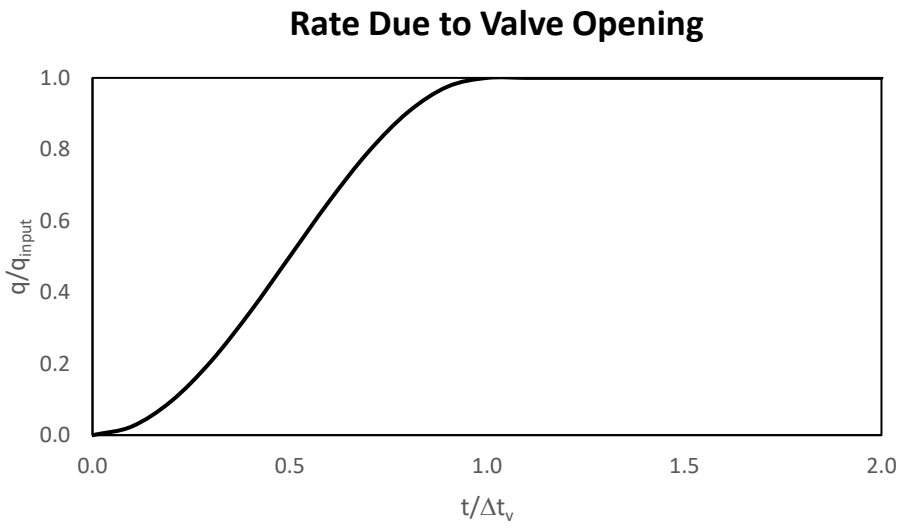

Figure 5.2. Rate variation due to valve opening.

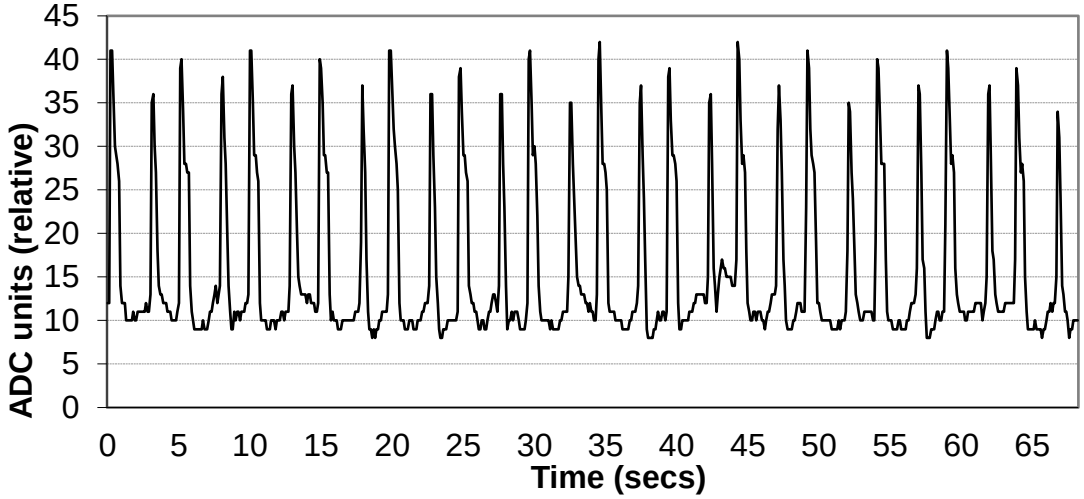

Figure 5.3 Tubing pressure variation measured on a beam pumping well (Pennebaker, 2014).

Chapter 6: Auxiliary Flow Equipment

Within the surface facilities a variety of flow equipment is needed to handle, transfer, and store produced fluids. These include tanks, flow junctions (i.e. headers), pumps, chokes, and compressors. In IFM these items are not modeled in detail internally but are represented as steady-state flow items.

FLOW JUNCTIONS

In general, the flow streams go to a junction, or header, where the flows are combined before being routed to a separator or other facility for treatment. Since the total volume of fluids within a header is usually very small compared to the flow rate through the header, steady-state flow within the header is assumed and pressure is assumed to be continuous, so that all incoming and outgoing streams will have the same pressure. Temperature is computed by performing a heat balance on the incoming streams to compute an average temperature, which is assigned to all of the outgoing streams. When more than one outgoing stream exist, the flow rates are divided equally among them. The equations describing the flow junction are as follows, where the index *i* represents inlets *1 ... n*, and j represents outlets *1 ... m*, and *p* represents the component or phase.

$$p_i = p_j, for\ all\ inlets\ i\ and\ outlets\ j \quad \text{.....(6.1)}$$

$$q_{pj}\rho_{p0} = \frac{1}{m}\sum_{i=1}^{n} q_{pi}\rho_{p0}\,, for\ each\ outlets\ j, each\ phase\ p \quad \text{.....(6.2)}$$

$$T_j = \frac{\sum_{i=1}^{n} T_i(q_{pi}\rho_{w0}c_{pw}c_{pg})}{\sum_{i=1}^{n}(q_{pi}\rho p_{w0}c_{po}c_{pg})}, for\ each\ outlets\ j \quad \text{.....(6.3)}$$

TANKS

Tanks are important for temporary storage of fluids within a field facility. Since the flow velocity is generally very slow and a tank normally has no outlet, only storage of fluids in the tanks is modeled in IFM. Pressure is assumed to be static and temperature is assumed to be uniform, representing a well-mixed fluid system at all times. As a result, the inlet pressure of the tank is equivalent to the static pressure head of fluids within the tank and will increase as the amount of fluids increases. In addition, the temperature is calculated by performing a heat balance on the tank fluids, plus the inlet fluids, accounting for heat loss to the environment.

SURFACE PUMPS

Pumps are needed to boost the pressure of fluids traveling through the facilities when the gravity head or well pressures are not adequate to allow flow through the entire facility. In IFM pumps are modeled as steady-state devices, where the mass through the pump is conserved. Each pump requires a performance relationship relating the flow rate and the pressure increment to the power requirements.

COMPRESSORS

Just as pumps are commonly used to move fluids through a facility, compressors are commonly used to move gases when the pressures are not adequate for processing requirements. In IFM compressors are modeled as steady-state devices, where a mass balance of fluids moving through the compressor is calculated. Due to the nature of gas, compression is always accompanied by an increase in temperature, which normally must be handled by cooling to avoid destruction of the compressor. Each compressor requires a performance relationship to relate the flow rate and pressure increase to the power requirements.

CHOKES

Chokes are used as control devices to limit flow and/or to reduce pressure in various parts of the flow system. Chokes are commonly used at wells to avoid problems with surges of fluids that may damage other equipment. In IFM chokes are modeled as steady-state devices with the pressure drop computed from the flow rate through the choke, given its orifice size. In addition, especially with gases, a temperature change may be observed. This is computed using an adiabatic heat balance of fluids entering and leaving the choke, but heat losses within the choke itself are not considered.

Chapter 7: Field Applications

Since the integrated field model has been developed and all of the parts have been validated, it is of interest to apply the model to actual field cases. As shown in Figure 7.1 the predicted and the measured dynamometers for a well with 20^{o} API oil are nearly identical, even though no tuning or damping factor was attempted in the predicted dynamometer card. Figure 7.2 also shows the predicted differences in dynamometer cards due to differing oil API gravity. Although not attempted here, it appears that IFM can be used to evaluate damping factors for use in damped wave equation applications by predicting the dynamometer with IFM, then fitting it with a damped wave equation.

Figure 7.3 shows the fluid level change as the pump runs, while Figure 7.4 shows the transient bottomhole pressure and oil flow rate from the reservoir influenced by the drop in the fluid level and bottomhole pressure. As can be seen, there is no indication that a stable pressure, flow rate or fluid level is achieved. Instead, fluctuations and transient effects appear to continue. In fact, longer detailed simulations show that the well remains in transient flow forever, since the pump strokes are shorter than the time needed for transients to be damped. This seems to bring into question the normal assumptions of constant rate and stable pump inlet pressure used in beam pump evaluations and designs. Further work on that subject appears to be warranted to validate that steady-state approximations can be used for design and diagnostics.

In most multi-well fields, flow from a number of wells goes to a flow junction, or header, where the flows are combined before being routed to a separator or other facility for treatment. To illustrate the effect of well interference through surface piping, a model shown in Figure 7.5 comprising two beam pumped wells producing into a common header was simulated. Pressure and rate fluctuations at the header are shown in Figures 7.6 and

7.7. Individual well fluctuations in pressure and rate are shown in Figure 7.8 and Figure 7.9. As can be seen, it appears that any assumption of steady-state flow is unwarranted, even in a simple two-well facility as shown in Figure 7.5.

- Damping Factor b = 0.6
- L = 4000 ft
- D_p = 2.5”
- D_r = 1”
- 10 SPM

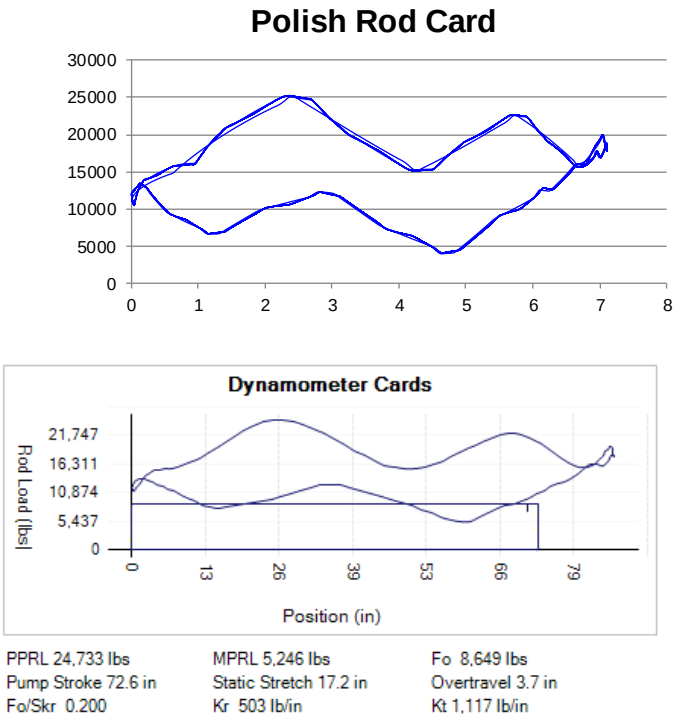

Figure 7.1. Predicted and measured dynamometer cards for 4,000 ft well.

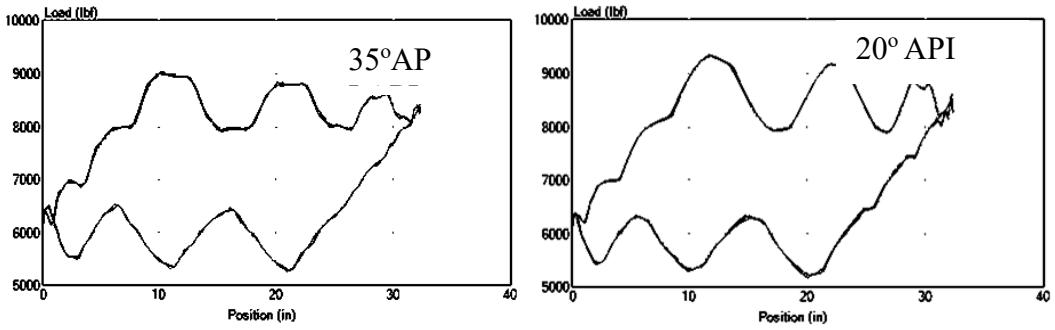

Figure 7.2. Predicted dynagraph for 4,000 ft well. Difference in dynamometer response due to differences in fluid density and viscosity, represented by API gravity differences.

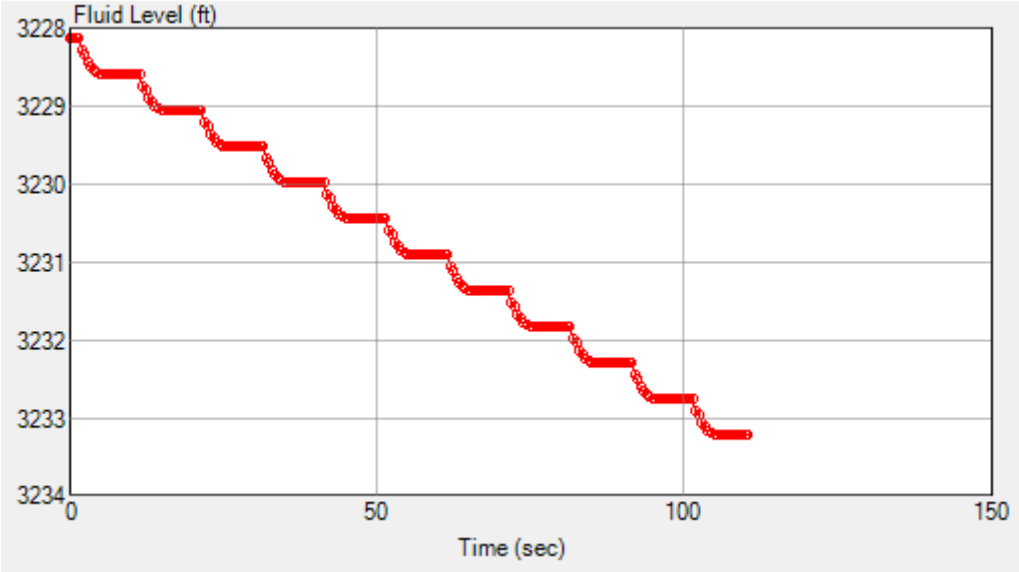

Figure 7.3. Predicted fluid level variation during startup of a beam pumped 4,000 ft well.

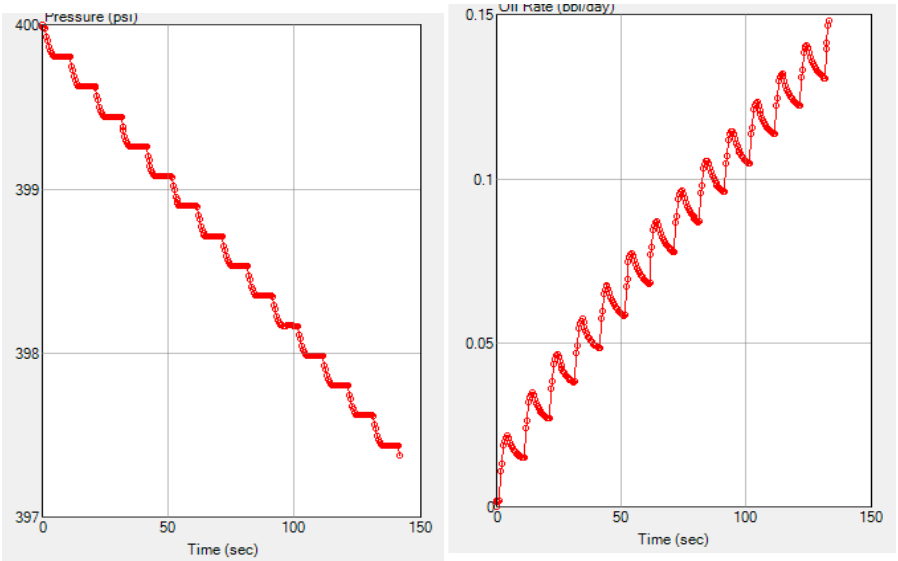

Figure 7.4. Predicted transient BHP and inflow rate for 4,000 ft well showing fluctuations as the pump starts.

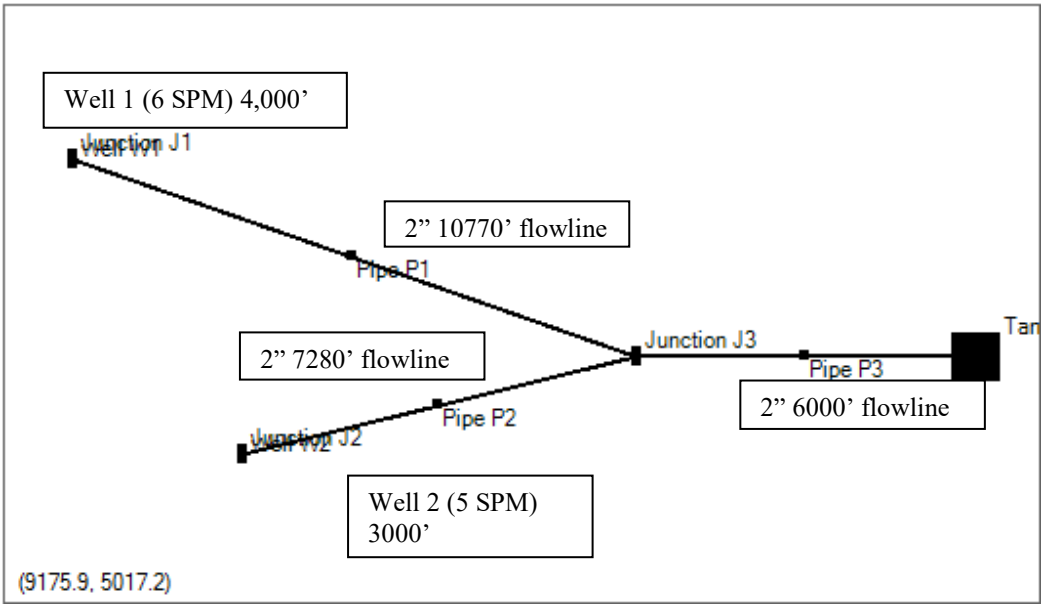

Figure 7.5. Comparison of measured and predicted dynamometers cards for 20 APIº and 4,000 ft well.

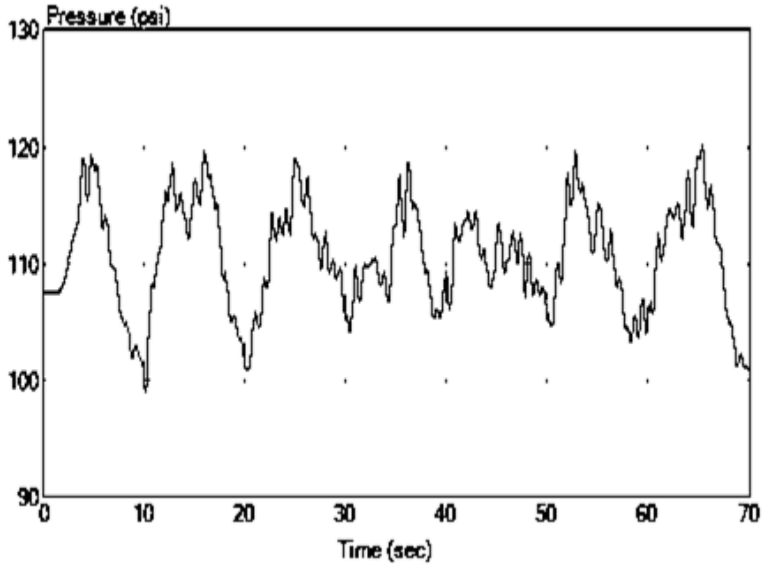

Figure 7.6. Predicted header pressure from example 2 well field.

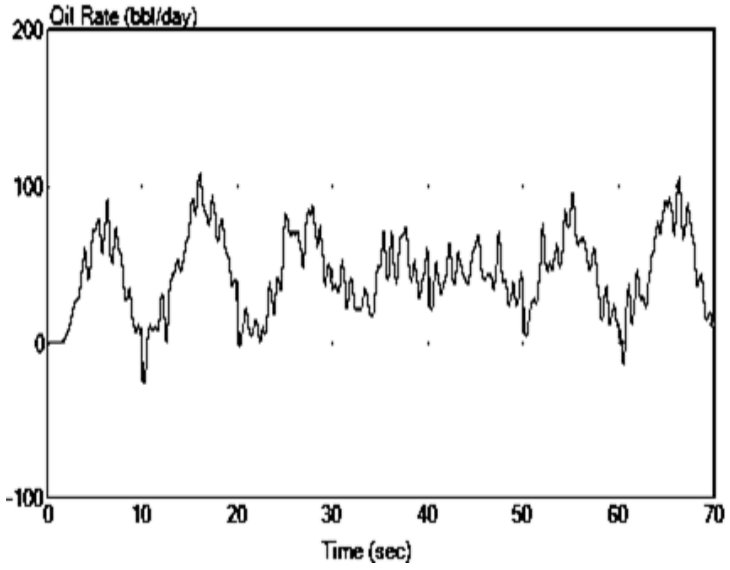

Figure 7.7. Predicted header flow rate from example 2 well field

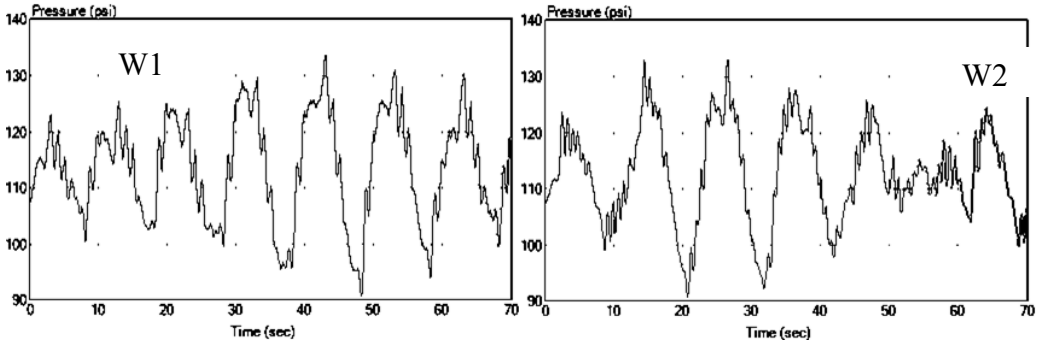

Figure 7.8. Predicted tubing pressure of wells in 2 well facility

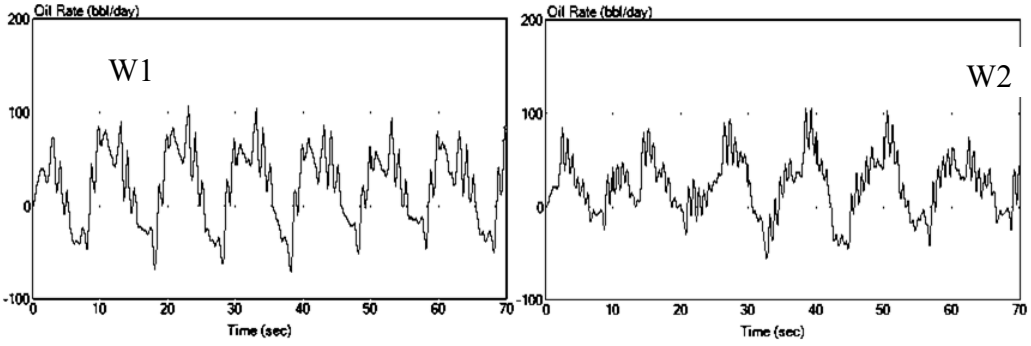

Figure 7.9. Predicted wellhead rate of wells in 2 well facility

Conclusions and Recommendations

As a result of the work documented in this dissertation, the following conclusions can be made and the following recommendations are made for future work.

CONCLUSIONS:

1) At the beginning of this work, it was doubtful that a complete field system could be modeled fully in transient flow, due to the difficulty in solving the nonlinear equations and the need for extremely small time steps for the surface equipment; however it is now concluded that it is feasible to model wells and simple facilities fully in transient flow.
2) Transient surface pressures exhibit complex behavior that may be chaotic.
3) As a result of the modeling work, it appears that common assumptions of steady-state flow in wells and facilities are largely unwarranted and should be reexamined when using simple analyses to estimate well performance and facility behaviors.
4) Interference between wells through the surface facilities is apparent. Therefore, interference-based analyses (interference tests, resistance capacitance models, etc.) should not assume that all interference is through the reservoir.

RECOMMENDATIONS:

1) The model can be used to evaluate the use of damping factors in existing damped wave equation software and analysis methods by generating dynamometer cards using IFM, then fitting them with a damped wave equation to determine the relationship between well and fluid properties and the apparent damping factors.

2) The annular flow model used in this dissertation is different from standard models, wherein a Reynolds number based on outer and inner radii is defined and friction factors are determined from experiment. Further theoretical and experimental work to further develop the superposition model used in this dissertation is justified.
3) Figure 7.4 shows how seemingly chaotic behavior can arise in even a simple oil field scenario. Chaos is defined by Hilborn et al. (1994) as a system that appears to have a random component, but is actually deterministic and controlled by nonlinear dynamics. The equations used in this dissertation are obviously nonlinear and should be capable of showing chaotic behavior as in Figure 7.4. It is known that chaotic systems tend to have solutions that follow an attractor in a suitable parameter space. IFM can be used to determine the parameter space and define the expected attractor. Then field measurements can be compared to the expected attractor. Measurements differing from the expected might be indicative of problems in the wellbore or surface facilities. This would provide a useful tool for field surveillance. IFM could also be used to illustrate what deviations are normal and arise from chaotic behavior and not from mechanical problems.
4) The IFM well models should be extended to include progressive cavity pumps, gas lift and electric submersible pumped wells.
5) Separator modeling in this dissertation is entirely empirical and should be reevaluated, perhaps using CFD (computational fluid dynamics) to justify the empirical approximations.
6) The rod coupling friction factors due to Valeev and Repin (1976) appear to be generally accepted and widely used in the literature but appear to be based on

scant data. It is recommended that their correlations be confirmed or modified using CFD.

7) In the literature, annular fluid flow is generally represented by defining a Reynolds Number based on inner and outer radii equivalent to a difference in Reynolds Numbers, then using experimental data to determine friction factors. The superposition approach used in this dissertation allows representing annular flow without experimental data but should be further evaluated with more theoretical and experimental analyses.

Appendices

APPENDIX A1: FLUID PROPERTIES

In the course of building a model of a reservoir, well, and surface equipment, the physical properties of fluids play an important role, since modeling the flow behavior of the system requires the use of density, viscosity, heat capacity, surface tension and other fluid properties. At times many of these properties are not directly measured and must be estimated. This section provides correlations and recommendations for estimating the fluid properties of interest in an integrated field model. It should be noted that when experimental or measured data is available, it should, of course, be used.

For reservoir and facilities calculations, it is generally required to model the flow of oil, gas and water mixtures. While other substances may at times be present (i.e. steam, polymer, sediments, etc.), these will not be represented in this section. In addition, complete equation of state modeling is possible in theory, but for inclusion in a complex integrated field model, the overhead of detailed flash calculations on top of the flow calculations is generally computationally infeasible. For that reason, a simplified black oil fluid model is used in IFM and is described here.

BLACK OIL PVT MODEL

The traditional black-oil PVT model is explained by Whitson and Brulé (2000) and consists of a three component, three phase fluid system. The components are oil, gas and water, corresponding to the fluids that are observed in the stock tank on the surface at standard conditions. The phases consist of a hydrocarbon liquid, a hydrocarbon vapor and an aqueous phase. It is assumed that there is no gas or oil in the aqueous phase, which therefore consists of only the water component. Furthermore, it is assumed that no water or oil exists in the hydrocarbon vapor phase, which therefore consists entirely of the gas

component. The hydrocarbon liquid phase, however, is assumed to consist of oil, along with the solution gas dissolved in the oil.

Note that neither the hydrocarbon vapor nor the aqueous phase requires a composition variable, since they consist only of a single component. The hydrocarbon liquid phase, however, consists of both oil and gas components; so a composition is needed to specify its properties. The composition variable is usually represented by the solution gas oil ratio, R_s, measured in standard cubic feet of gas per stock tank barrel of oil. To completely specify the state of a black-oil fluid, it is necessary to specify the oil, gas and water components, as well as the temperature, pressure and solution gas-oil ratio.

In the following sections, properties of the hydrocarbon liquid, hydrocarbon gas and aqueous phases are estimated. Note that there are several commonly used parameters that can be derived from the basic parameters. For example, in IFM the isothermal compressibility and thermal expansion factors of all fluids are computed from density to maintain consistency and enthalpy is computed from heat capacity, temperature and density.

$$c_f = \frac{1}{\rho_f}\frac{\partial \rho_f}{\partial p},\ c_{fT} = -\frac{1}{\rho_f}\frac{\partial \rho_f}{\partial T},\ h_f = U + pV \quad \text{.....(A1.1)}$$

Where

c_f = isothermal compressibility

ρ_f = fluid density (lb/ft^3)

p = pressure (psia)

c_{fT} = thermal expansion factor

h_f = fluid enthalpy

T = temperature (°F)

U = internal energy

V = volume

BRINE

The properties of pure water have been extensively studied and are available in the literature. Since oil field waters are generally not pure; representing the effect of impurities, primarily sodium chloride salt, are important. In some cases, detailed water analyses may be available and should be used if possible. A summary of many properties of oil field waters is given in McCain Jr (1991).

Composition

The composition of oil field waters varies from nearly pure water to salt saturated brines. Quite often only a general description of the composition is given as total dissolved solids expressed in weight or volume percent or in parts per million (ppm) of water or of total brine. In IFM weight percent of total dissolved solids (TDS) is used exclusively. The weight fraction can be computed for other measures as described by Whitson (2000).

$$\begin{aligned} w_s = &\quad (ppm\ TDS)\ 10^{-6} \\ w_s = &\quad (wt\ \%)\ 10^{-2} \end{aligned} \quad \text{.....(A1.2)}$$

Density

Brine density at standard conditions, when not measured, can be estimated from the Rowe-Chow density correlation for sodium chloride solutions. (Rowe Jr and Chou (1970)). For use in IFM a factor of 1.0009 has been added so that at standard conditions the correct water density is obtained for pure water ($w_s = 0$).

$$\rho_{wsc} = \frac{1.0009(62.37)}{1.0009 - 0.71\, w_s + 0.26055\, w_s^2} \quad \text{.....(A1.3)}$$

For other pressures and temperatures, the density is estimated using the formation volume factor using the definition of formation volume factor.

$$\rho_w = \frac{\rho_{wsc}}{\boldsymbol{B_w}} \quad \text{.....(A1.4)}$$

Formation Volume Factor

The water formation volume factor and compressibility will generally depend upon the amount of dissolved gas, as well as temperature, pressure and salinity. In IFM the effect of solution gas in water is ignored. The formation volume factor for brines from the correlation by McCain Jr (1990) as reported by Bánzer S. (1996) is used in IFM. The equation is as follows.

$$\Delta V_{wT} = -1.0001 \times 10^{-2} + 1.33391 \times 10^{-4} T + 5.50654 \times 10^{-7} T^2$$

$$\Delta V_{wp} = -1.95301 pT \times 10^{-9} - 1.72834 \times 10^{-13} p^2 T - 3.58922 \times 10^{-7} p - 2.25341 \times 10^{-10} p^2$$

$$B_w = (1 + \Delta V_{wp})(1 + \Delta V_{wT}) \quad \text{(A1.5)}$$

Viscosity

Water viscosity can be estimated from several correlations; however, in IFM the correlation of McCain Jr (1990) as reported by Bánzer S. (1996) is used. The equation is as follows.

$$A = 109.574 - 0.0840564 w_s + 0.00313314 {w_s}^2 + 0.0000872213 {w_s}^3$$

$$B = -1.12166 + 2.63951 \times 10^{-4} w_s - 6.79461 \times 10^{-6} {w_s}^2 - 5.47119 \times 10^{-7} {w_s}^3 + 1.55586 \times 10^{-8} {w_s}^4$$

$$C = 0.9994 + 4.0295 \times 10^{-5} p + 3.1062 p^2$$

$$\mu_w = C\, A\, T^B \quad \text{(A1.6)}$$

where

T= temperature (F)

w_s=weight fraction solid

p = pressure (psia)

B, C factors used in correlation as shown.

Heat Capacity

The heat capacity of water has been presented by Holman (1958) and is valid over the range of 20 °C to 290 °C (68 °F to 554 °F).

$$C_{pw} = \frac{4245 - 1.841\,T[K]}{\rho_w[gm/cm^3]}\left(\frac{J}{kg \cdot K}\right) = \frac{70.1725 - 0.015254\,T[F]}{\rho_w[lbm/ft^3]}\left(\frac{BTU}{lbm \cdot F}\right) \quad \text{(A1.7)}$$

OIL

The correlations presented here are for the oil phase of a black oil model. As such it is important to remember that the oil properties must account for the dissolved gas.

Density

Oil density at standard conditions is usually reported as API gravity. The actual density in lb/ft^{3}can be calculated from the definition of API gravity as follows.

$$\rho_{osc} = 62.37\left(\frac{131.5 + \gamma_{API}}{141.5}\right) \quad \text{(A1.8)}$$

Where

API, γ_{API}= API gravity (degrees API).

For other pressures and temperatures, the density is estimated with the formation volume factor using the definition of formation volume factor. Note that the solution gas is accounted for by using the gas density and standard conditions and the solution gas-oil ratio:

$$\rho_0 = \frac{\rho_{0sc} + 5.6146 R_s \rho_{gsc}}{\boldsymbol{B_o}} \quad \text{(A1.9)}$$

Formation Volume Factor

The water formation volume factor will generally depend upon the amount of dissolved gas, as well as temperature, pressure and the oil and gas component properties.

In IFM the correlation of Standing (1977) is used. The equation to estimate the formation volume factor at the bubble point pressure is.

$$B_{ob} = 0.9759 + 1.2 \times 10^{-5} \left[R_s \sqrt{\frac{\gamma_g}{\gamma_o}} + 1.25T \right]^{1.2} \quad \text{(A1.10)}$$

Above the bubble point pressure, the formation volume factor depends upon the oil compressibility. Given the compressibility of the undersaturated fluid above the bubble point pressure, the formation volume factor is calculated by the following relation.

$$B_o = B_{ob} e^{c_o (p - p_b)} \quad \text{(A1.11)}$$

Solution Gas-Oil Ratio

The solution gas-oil ratio for a saturated oil is estimated from Standing's correlation. Note that the relation may be solved either for solution gas-oil ratio or for bubble point pressure as presented in Standing (1977). We note that if there is free gas present, the oil is assumed to be saturated and at its bubble point, so the following correlation for the solution gas-oil ratio should be used.

Note that Standing's correlations do not apply to surface conditions, since they do not approach the correct values at standard pressure and temperature

$$p_b = 18.2 \left[\left(\frac{R_{sb}}{\gamma_g} \right)^{0.83} 10^{0.00091\, T - 0.0125\, API} - 1.4 \right] \quad \text{(A1.12)}$$

$$R_{sb} = \gamma_g \left[\left(\frac{p_b}{18.2} + 1.4 \right) 10^{-0.00091\, T + 0.0125\, API} \right]^{1/0.83} \quad \text{(A1.13)}$$

Viscosity

Oil viscosity is usually estimated in two or three steps. First the dead oil viscosity is estimated, then the value is modified to account for solution gas as well as temperature at the bubble point pressure. Finally, if the oil is above the bubble point, an additional correction is used to account for the higher pressure. In IFM the Beggs and Robinson

(1975) correlation for dead oils and saturated crudes is used, while the correlation of Beal (1946) as fit by Standing (1977) is used to correct for pressures above the bubble point pressure. The equations are as follows.

$$\mu_{od} = 10^{10^{3.0324-0.02023\,API}\,T^{-1.163}} - 1$$

$$\mu_{ob} = \frac{10.715}{(R_s + 100)^{0.515}}\ \mu_{od}^{\frac{5.44}{(R_s+150)^{0.338}}}$$

$$\mu_o = \mu_{ob} + \left(0.024{\mu_{ob}}^{1.6} + 0.038{\mu_{ob}}^{0.56}\right)\left(\frac{p-p_b}{1000}\right) \quad \text{(A1.14)}$$

Heat Capacity

Gambill (1957) presented the following correlation for heat capacity and it is used in IFM.

$$\mathrm{C_{po}} = \frac{0.388+0.00045\,\mathrm{T}}{\sqrt{\gamma_o}} \quad \text{(A1.15)}$$

GAS

Most volumetric properties of hydrocarbon gases can be estimated using the real gas equation of state as explained in Whitson (2000). For reference the real gas equation of state is

$$pV = znRT \quad \text{(A1.16)}$$

To use this equation, the z-factor must be determined, and the usual method correlates the z-factor using corresponding states as a function of reduced temperature and reduced pressure, which depend on the actual temperature and pressure relative to the pseudo-critical temperature and pressure respectively.

The pseudo-critical temperature and pressure can be estimated from compositional data; however, in many cases compositional data is not available, so the following correlations are used as given in Standing (1977). For reference, the definition of the

pseudo-reduced properties is also given. It should be remembered that absolute temperature is required in all gas equations. Degrees Rankine (R) is used here.

$$T_{pc} = 706 - 51.7\,\gamma_g - 11.1\gamma_g^2 \quad \text{(Al.17)}$$

$$p_{pc} = 187 + 330\,\gamma_g - 71.5\gamma_g^2 \quad \text{(A1.18)}$$

$$T_{pr} = \frac{T}{T_{pc}}\ and\ p_{pr} = \frac{p}{p_{pc}} \quad \text{(A1.19)}$$

Z Factor

The z-factor for hydrocarbon gases is estimated using an iterative solution to the equation of state presented by Hall and Yarborough (1973).

$$z = \frac{p_{pr}}{y},\ t = \frac{1}{T_{pr}},\ a = 0.06125te^{-1.2(1-t)^2} \quad \text{(A1.20)}$$

The z-factor is found by search for the root, *y*, of the following equation:

$$f(y) = 0 = ap_{pr} + \frac{y + y^2 + y^3 - y^4}{(1-y)^3} - (14.76t - 9.76t^2 + 4.58t^3)y + (90.7t - 242.2t^2 + 42.4t^3)y^{1.18+2.82t} \quad \text{(A1.21)}$$

Density

Gas density at standard conditions is usually computed from the gas specific gravity relative to air. Since the standard density of air is 0.0763 lb/ft^3, the gas density at standard conditions is simply 0.0763 and it can be calculated from the definition of specific gravity as follows.

$$\rho_{gsc} = 0.0763\gamma_g \quad \text{(A1.22)}$$

For other pressures and temperatures, the density is estimated using the real gas equation of state with a z-factor computed as described above.

$$\rho_g = \rho_{gsc}\frac{pT_{std}}{\boldsymbol{zTp_{std}}} \quad \text{(A1.23)}$$

Formation Volume Factor

The gas formation volume factor is also calculated from the real gas equation of state using a z-factor as described above. Using the equation, the ratio of reservoir to standard volumes for a gas is given by the following equation.

$$B_g = \frac{z\, p_{std}\, T}{p\, T_{std}} \quad \text{(A1.24)}$$

Viscosity

Gas viscosity is rarely measured in the laboratory and is normally estimated from correlations. In IFM, the Lee et al. (1966) correlation is used. The equations are as follows.

$$A_1 = \frac{(9.379 + 0.01607M)T^{1.5}}{209.2 + 19.26M + T}, \qquad A_2 = 3.448 + \frac{986.4}{T} + 0.01009M$$

$$A_3 = 2.447 - 0.2224\, A_2$$

$$\mu_g = \frac{A_1}{10000} e^{A_2 \rho_g^{A_3}} \quad \text{(A1.25)}$$

Heat Capacity

Gambill (1957) presented the following correlation for heat capacity that is used in IFM.

$$\mathrm{C_{po}} = \frac{1684 + 3.389\ \mathrm{T[K]}}{\sqrt{\gamma_o}} \left(\frac{\mathrm{J}}{\mathrm{kg \cdot K}}\right) = \frac{4.80976 + 0.003552\ \mathrm{T[F]}}{\sqrt{\rho_o [\mathrm{lbm/ft^3}]}} \left(\frac{\mathrm{BTU}}{\mathrm{lbm \cdot F}}\right) \quad \text{(A1.26)}$$

APPENDIX A2: PARAMETER ESTIMATION

In the previous section the representation and estimation of fluid properties was presented. Besides fluid properties, many additional parameters are required for modeling integrated systems. These include heat loss coefficients, as well as equipment specifications and efficiencies. Unfortunately, many of these properties are rarely measured directly and must be estimated. Even in the case of equipment specifications, where manufacturers' specification sheets may be available, the specifications usually give minimum performance and maximum limits for new equipment. Since many marginal fields make use of used or old equipment, de-rating must often be applied to determine the actual equipment performance. This section provides correlations and recommendations for estimating many of the parameters required for full system modeling. Fluid properties are covered in a preceding appendix. It should be noted that when valid manufacturers' data sheets are available, they should be used as a guideline and when experimental or measured data is available, it should be used. In many cases values will need to be adjusted to match observed field performance.

HEAT TRANSFER COEFFICIENTS

In general, heat transfer is modeled using the standard equation for heat flow following the development in Prats (1986) shown as Equation A2.1, where $Q/\Delta L$ is the rate of heat loss per unit length, R_h is the specific thermal resistance in $(BTU/ft^2\text{-}D\text{-}°F)^{-1}$, and ΔT is the temperature difference between the equipment and the environment. Note that in this equation the loss of heat from the equipment is positive when the equipment temperature is greater than the environment temperature, so that ΔT is positive. Prats (1986)

also provides information on calculating heat losses from insulated pipes and contains material properties for estimating thermal parameters for a variety of materials.

$$Q/\Delta L = \Delta T/R_h \quad \text{.....(A2.1)}$$

Following Prats' development, it is assumed that the pipes consist of internal scale, metal pipe wall, an external scale coating, and an insulation coating. Outside the pipe forced convection of air may also be considered for raised pipes or heat loss to the surrounding soil if the pipe is buried. Note that Prats also includes a laminar film for steam laden pipes, but that is ignored in this development and it is assumed that liquid coats the inside of the pipes and is at the fluid temperature. Under those constraints the composite thermal resistance is given by:

$$R_h = \frac{1}{2\pi}\left[\frac{1}{h_{Pi}r_i} + \frac{1}{\lambda_P}\ln\frac{r_o}{r_i} + \frac{1}{h_{Po}r_o} + \frac{1}{\lambda_{ins}}\ln\frac{r_{ins}}{r_o} + \frac{1}{h_{fc}r_{ins}}\right] \quad \text{.....(A2.2)}$$

where λ_P and λ_{ins} represent the thermal conductivity of the pipe and insulation, h_{Pi} and h_{Po} represent the heat transfer coefficient across the inner and out scale deposits, and h_{fc} accounts for heat transfer due to forced convection from outside the pipe. Note that heat radiation is ignored, since the temperature at the outside surface is usually not large. For most purposes, it can also be assumed that the contact between the inside and outside scale deposits and the pipe are good, so those respective terms can be ignored, resulting in the following equation.

$$R_h = \frac{1}{2\pi}\left[\frac{1}{\lambda_P}\ln\frac{r_o}{r_i} + \frac{1}{\lambda_{ins}}\ln\frac{r_{ins}}{r_o} + \frac{1}{h_{fc}r_{ins}}\right] \quad \text{.....(A2.3)}$$

Note that for uninsulated pipe, $r_{ins}/r_o = 1$ and the logarithm term becomes zero.

From table B.9 in Prats (1986), the thermal conductivity of carbon steel is about 600 BTU/D-ft-°F and the thermal conductivity of insulation may be in the range of 1 – 10 BTU/D-ft-°F. According to Prats(1986), the heat transfer coefficient for forced convection due to wind is estimated as:

$$h_{fc} = \frac{18}{r_e}(r_e v_w)^{0.6} \text{(BTU/D-ft-°F)} \quad \text{(A2.4)}$$

where v_w is the wind velocity normal to the pipe in mi/hr and r_e is the radius exposed to air in ft.

References

Aho, A.V., Hopcroft, J.E. and Ullman, J.D. 1983 *Data Structures and Algorithms*, Addison-Wesley Publishing Company.

Arnold, K. and Stewart, M. 1999 *Surface Production Operations, Volume 1, Design of Oil Handling Systems and Facilities*, Butterworth-Heinemann.

Bánzer S., C. 1996 *Correlaciones Numéricas P. V. T.*, Maracaibo, Venezuela: Universidad de Zulia.

Barreto Filho, M. de A. 2001 'Estimation of Average Reservoir Pressure and Completion Skin Factor of Wells that Produce Using Sucker Rod Pumping', University of Texas at Austin

Beal, C. 1946 'The viscosity of air, water, natural gas, crude oil and its associated gases at oil field temperatures and pressures', *TP* 2018, 94–115

Beggs, H.D. and Robinson, J.R. 1975 'Estimating the viscosity of crude oil systems', *Journal of Petroleum technology* 27, 1140–41

Bergant, A., Ross Simpson, A. and Vìtkovsk, J. 2001 'Developments in unsteady pipe flow friction modelling', *Journal of Hydraulic Research* 39, 249–57

Bird, R.B., Stewart, W.E. and Lightfoot, E.N. 2007 *Transport Phenomena*, (Second Edition,). New York, NY: John Wiley & Sons, Inc.

Brill, J.P. and Mukherjee, H. 1999 *Multiphase Flow in Wells*, Vol 17 Richardson, TX: Monograph Series, SPE.

Chisholm, D. 1967 'A theoretical basis for the Lockhart-Martinelli correlation for two-phase flow', *International Journal of Heat and Mass Transfer* 10, 1767–78

Csaszar, A.B., Laine, R.E., Keating, J.F. and Jennings, J.W. 1991 'Sucker-Rod Pump Diagnosis With Fluid Inertia Considerations', in *SPE Production Operations Symposium*Society of Petroleum Engineers.

Daugherty, R.L. and Franzini, J.B. 1965 *Fluid mechanics with engineering applications*, . New York: McGraw-Hill.

Doty, D.R. and Schmidt, Z. 1983 'An improved model for sucker rod pumping', *Soc. Pet. Eng. AIME, Pap.;(United States)* 23,

Earlougher, R.C. 1977 'Monograph vol. 5: Advances in Well Test Analysis', *Society of Petroleum Engineers* 90–104

Everitt, T.A. and Jennings, J.W. 1992 'An improved finite-difference calculation of downhole dynamometer cards for sucker-rod pumps', *SPE production engineering* 7, 121–27

Frankiewicz, T. and Lee, C.-M. 2002 'Using Computational Fluid Dynamics (CFD) Simulation to Model Fluid Motion in Process Vessels on Fixed and Floating Platforms', in *SPE Paper 77494*. San Antonio, TX.:

Gambill, W.R. 1957 'You Can Predict Heat Capacities', *Chemical Engineering* 243–48

Gibbs, S.G. 1963 'Predicting the Behavior of Sucker-Rod Pumping Systems', *Journal of Petroleum Technology* 15,

Gibbs, S.G. and Neely, A.B. 1966 'Computer diagnosis of down-hole conditions in sucker rod pumping wells', *Journal of petroleum technology* 18, 91–98

Govier, G.W. and Aziz, K. 2008 *The Flow of Complex Mixtures in Pipes*, (2nd Edition,). Richardson, TX: Society of Petroleum Engineers.

Gray, H.E. 1963 'Kinematics of Oil-Well Pumping Units', *Drilling and Production Practice*

Hafskjols, B., Celius, H.K. and Aamo, O.M. 1999 'A New Mathematical Model for Oil/Water Separation in Pipes and Tanks', *SPE P&F* 14, 30–36

Hall, K.R. and Yarborough, L. 1973 'A new equation of state for Z-factor calculations', *Oil and Gas journal* 71, 82–92

Hallinger, A., Soenstaboe, F. and Knutsen, T. 1996 'A Simulation Model for Three-Phase Gravity Separators', in *SPE Paper 36644*. Denver, CO:

Hilborn, R.C., Coppersmith, S., Mallinckrodt, A.J. and McKay, S. 1994 'Chaos and nonlinear dynamics: an introduction for scientists and engineers', *Computers in Physics* 8, 689–689

Himmelblau, D.M. and Bischoff, K.B. 1968 *Process Analysis and Simulation: Deterministic Systems*, . New York, NY: John Wiley & Sons, Inc.

Holman, J.P. 1958 *Heat Transfer*, (4th Edition,). New York, NY: McGraw-Hill Book Co.

IOGCC 2008 *Marginal Wells: Fuel for Economic Growth*, Interstate Oil and Gas Compact Commission.

Kolev, N.I. 2002 *Multiphase Flow Dynamics 1, Fundamentals*, . Berlin: Springer-Verlag.

Langston, L.V. 2003. 'The Lease Pumper's Handbook, First Edition'

Lee, A., González, M. and Eakin, B. 1966 'The viscosity of natural gases', *Journal of Petroleum Technology* 18, 997–1000

Lekia, S.D.L. (Unocal P. and D.T. and Evans, R.D. (Univ of O. 1995 'A Coupled Rod and Fluid Dynamic Model for Predicting the Behavior of Sucker-Rod Pumping Systems. Part 1: Model Theory and Solution Methodology', *SPE Production and Facilities (Society of Petroleum Engineers); (United States)* 10:1,

Lockhart, R.W. and Martinelli, R.C. 1949 'Proposed Correlation of Data for Isothermal Two-Phase, Two-Component Flow in Pipes', *Chemical Engineering Progress* 45, 39–48

McCain Jr, W.D. 1990 *The Properties of Petroleum Fluids*, Tulsa, OK: PennWell Books.

McCain Jr, W.D. 1991 'Reservoir-Fluid Property Correlations—State of the Art', *SPE Reservoir Engineering*

Minami, K. 1991 'Transient Flow and Pigging Dynamics in Two-Phase Pipelines', The University of Tulsa

Minami, K. and Shoham, O. 1994 'Transient two-phase flow behavior in pipelines-experiment and modeling', *International journal of multiphase flow* 20, 739–52

Pennebaker, S. 2014. 'Personal Communication'

Prats, M. 1986 *Thermal Recovery, volume 7 of SPE Monograph Series*, Society of Petroleum Engineers.

RELAP5 2012 *RELAP5-3D© Code Manual Volume I: Code Structure, System Models and Solution Methods*, Idaho National Laboratory.

Rosso, F. and Sona, G. 2001 'Gravity-driven separation of oil-water dispersions', *Advances in Mathematical Sciences and Applications* 11, 127–51

Rowe Jr, A.M. and Chou, J.C. 1970 'Pressure-volume-temperature-concentration relation of aqueous sodium chloride solutions', *Journal of Chemical and Engineering Data* 15, 61–66

Schafer, D.J. and Jennings, J.W. 1987 'An investigation of analytical and numerical sucker rod pumping mathematical models', in *SPE Annual Technical Conference and Exhibition*Society of Petroleum Engineers.

Shirdel, M. 2010 ‘Development of a Coupled Wellbore-Reservoir Compositional Simulator for Horizontal Wells’, MS Thesis, University of Texas

Shirdel, M. 2013 ‘Development of a Coupled Wellbore-Reservoir Compositional Simulator for Damage Prediction and Remediation’, University of Texas at Austin

Shoham, O. 2006 *Mechanistic Modeling of Gas-Liquid Two-Phase Flow in Pipes*, . Richardson, TX: Society of Petroleum Engineers.

Song, J.H., Jeong, B.E., Kim, H.J. and Gil, S.S. 2010 ‘Three-Phases Separator Sizing Using Drop Size Distribution’, in *OTC Paper 20558*. Houston, TX:

Standing, M.B. 1977 *Volumetric and Phase Behavior of Oil Filed Hydrocarbon Systems*, . Dallas, TX: SPE of AIME.

Taitel, Y. and Dukler, A.E. 1976 ‘A model for predicting flow regime transitions in horizontal and near horizontal gas-liquid flow’, *AIChE Journal* 22, 47–55

Valeev, M.D. and Repin, N.N. 1976 ‘IZVESTIYA VYSSHIKH VCHEBNYKH ZAVEDENII’, *NEFT I GAZ* 8, 33–44

Whitson, C.H. and Brulé, M.R. 2000 *Phase Behavior*, Vol 20 Richardson, TX: Monograph Series, SPE.

Xu, J., Doty, D.R., Blais, R., Shahraki, A. and Lea, J. 1999 ‘A comprehensive rod-pumping model and its applications to vertical and deviated wells’, in *SPE mid-continent operations symposium* 637–45